Nonlinear Large Deflection Theory with Modified Aeroelastic Lifting Line Aerodynamics for a High Aspect Ratio Flexible Wing

Nhan Nguyen *
NASA Ames Research Center, Moffett Field, CA 94035
Eric Ting †
NASA Ames Research Center, Moffett Field, CA 94035
Daniel Chaparro ‡
Stinger Ghaffarian Technologies, Inc., Moffett Field, CA 94035

This paper investigates the effect of nonlinear large deflection bending on the aerodynamic performance of a high aspect ratio flexible wing. A set of nonlinear static aeroelastic equations are derived for the large bending deflection of a high aspect ratio wing structure. An analysis is conducted to compare the nonlinear bending theory with the linear bending theory. The results show that the nonlinear bending theory is length-preserving whereas the linear bending theory causes a non-physical effect of lengthening the wing structure under the no axial load condition. A modified lifting line theory is developed to compute the lift and drag coefficients of a wing structure undergoing a large bending deflection. The lift and and drag coefficients are more accurately estimated by the nonlinear bending theory due to its length-preserving property. The nonlinear bending theory yields lower lift and span efficiency than the linear bending theory. A coupled aerodynamic-nonlinear finite element model is developed to implement the nonlinear bending theory for a Common Research Model (CRM) flexible wing wind tunnel model to be tested in the University of Washington Aeronautical Laboratory (UWAL). The structural stiffness of the model is designed to give about 10% wing tip deflection which is large enough that could cause the nonlinear deflection effect to become significant. The computational results show that the nonlinear bending theory yields slightly less lift than the linear bending theory for this wind tunnel model. As a result, the linear bending theory is deemed adequate for the CRM wind tunnel model.

I. Introduction

Modern aircraft are increasingly designed to be highly aerodynamically efficient in order to reduce the fuel consumption, hence operating cost of modern transports. To achieve this goal, the aircraft industry has been adopting a high aspect ratio wing design with the advanced composite construction in modern transports. Aircraft design concepts that take advantage of wing flexibility to increase aerodynamic performance and maneuverability have been investigated. By twisting a wing structure, an aerodynamic moment can be generated to enable an aircraft to execute a maneuver in lieu of the traditional flight control surfaces. For example, a rolling moment can be induced by twisting the left and right wings in the opposite direction. Similarly, a pitching moment can be generated by twisting both wings in the same direction. Wing twisting or warping for flight control is not a new concept and was used in the Wright Flyer in the 1903. The U.S. Air Force conducted the Active Flexible Wing program in the 1980's and 1990's to explore the potential use of leading edge slats and trailing edge flaps to increase the control effectiveness of F-16 aircraft for high speed

*NASA Ames Research Center, Research Scientist, AIAA Associate Fellow, nhan.t.nguyen@nasa.gov
†NASA Ames Research Center, Research Engineer, eric.b.ting@nasa.gov
‡Stinger Ghaffarian Technologies Inc., NASA Ames Research Center, Research Engineer, daniel.chaparro@nasa.gov

maneuvers.[1] In the 2000's, the Active Aeroelastic Wing research program also investigated a similar wing twisting technology for improved roll maneuverability of a modified F/A-18 aircraft.[2] Wing shaping control concepts for drag reduction are being studied by NASA to leverage wing flexibility for aerodynamic performance.[3,4] By re-twisting a flexible wing and using variable camber aerodynamic flight control surfaces, aircraft wings can have a mission-adaptive capability to optimize L/D throughout a flight envelope.[5] In recognition of the role of aeroelasticity on aircraft performance and dynamics, NASA Advanced Air Transport Technology (AATT) project is conducting research in the area of Performance Adaptive Aeroelastic Wing (PAAW). This research develops concepts such as the variable camber continuous trailing edge flap (VCCTEF) to enable wing shaping control for aerodynamic performance and dynamics.[3,6] Currently, a wind tunnel test is being planned to conduct an active real-time drag minimization control strategy for a high aspect ratio flexible wing based on the Common Research Model[7] equipped with the VCCTEF in the University of Washington Aeronautical Laboratory (UWAL). The wing is purposely designed with a reduced structural stiffness to achieve about a 10% wing tip deflection. Efforts are under way to create an aerodynamic-structural model of this wind tunnel model. It is of interest to investigate the effect of nonlinear large deflection bending on this wind tunnel model so that a better understanding can be ascertained prior to the wind tunnel test entry.

Structural deflections of lifting surfaces interact with aerodynamic forces to create aeroelastic coupling that can affect aircraft performance. Understanding these effects can improve the prediction of aircraft performance and provide an insight into how to design an aerodynamically efficient high aspect ratio flexible wing. Generally, high aspect ratio lifting surfaces undergo a greater degree of structural deflections than low aspect ratio lifting surfaces. As a result, the nonlinear structural deflection could have a significant effect on the aerodynamic performance.

The purpose of this study is to investigate the effect of nonlinear large deflection bending on the high aspect ratio CRM flexible wing to ascertain whether or not this effect should be given further consideration in the analysis of the wind tunnel test data and future optimization efforts. Toward this end, a nonlinear bending theory is developed along with a modified lifting line theory which includes the effect of the wing aeroelastic deflections. A nonlinear finite element model is developed to implement the nonlinear bending theory. The finite element model is then coupled to an aerodynamic model of the CRM wing which is based on a vortex lattice method with transonic and viscous corrections via a 2D transonic small disturbance method[9] and a 2D integral boundary layer method.[10] The coupled aerodynamic-nonlinear finite element model is analyzed to quantify the aerodynamic performance of this model.[8]

II. Common Research Model

The aerodynamic model is a wind tunnel sub-scale model of a CRM wing to be tested in the UWAL in 2017 to demonstrate an active real-time drag optimization control strategy. This CRM model is designed to have about 10% wing tip deflection to represent the current state of the art high aspect ratio wings in modern transport aircraft such as the Boeing 777. The model is 85 inches in length with an elastic axis sweep angle of 31.5° and includes six active two-segment VCCTEF control surfaces as shown in Fig. 1. These surfaces are driven by actuators for the real-time drag minimization control strategy. The test conditions are at low subsonic speed of about Mach 0.1.

An aerodynamic model of this CRM wing is constructed using NASA vortex lattice code VORLAX. A transonic correction has been developed for VORLAX to account for transonic flow over wings. The transonic correction is based on the transonic small disturbance (TSD) theory[9] and is implemented using a 2D transonic code TSFOIL developed by NASA Ames Research Center.[9] For the wind tunnel model analysis, the transonic correction is not needed, but for a full-scale CRM model, this correction will be required. In addition, the viscous effect is also corrected for in VORLAX via a 2D integral boundary layer code developed in-house by NASA Ames Research Center.[10] The coupled transonic plus integral boundary layer method with the vortex lattice method has been shown to be able to produce reasonably accurate aerodynamic performance prediction as compared to a Reynolds-Averaged Navier-Stokes (RANS) CFD solver which is computationally much more expensive than the vortex lattice method.[9] Moreover, the vortex lattice code VORLAX has the mesh deformation capability that allows it to be easily coupled to a finite element model for static aeroelastic analysis,[11] whereas the mesh deformation capability is only available for a few NASA RANS CFD solvers. With the nonlinear finite element capability, the coupling will require more iterations for a solution to converge. Thus, this will create an additional computational cost that must be taken into account

for RANS solvers, whereas such cost is very small for the vortex lattice method even with the transonic and viscous corrections. For conceptual aerodynamic analyses and multidisciplinary design optimization, this method is very computationally efficient and can generate rapid candidate design solutions.

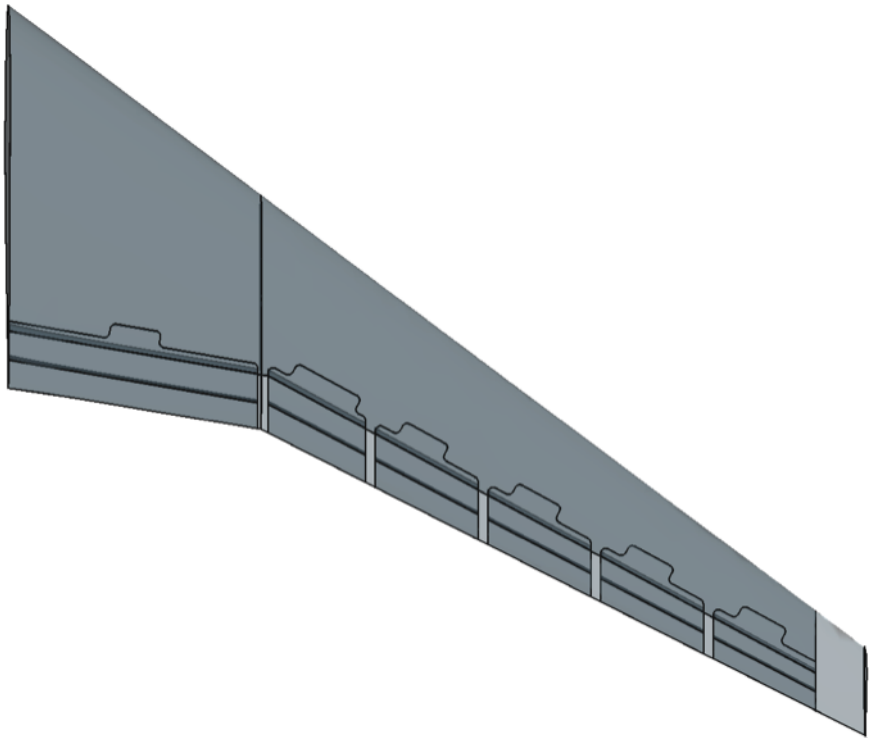

Figure 1. Common Research Model Sub-Scale Wind Tunnel Model in UWAL

Figure 2 shows the surface pressure distribution of the full-scale CRM wing at Mach 0.85 and Reynolds number of 1.88 million per foot. The model shows a transonic region in the wing root area as is typically the case with transport wings. Figures 3 and 4 shows the computed lift curve and drag polar of the CRM rigid wing.

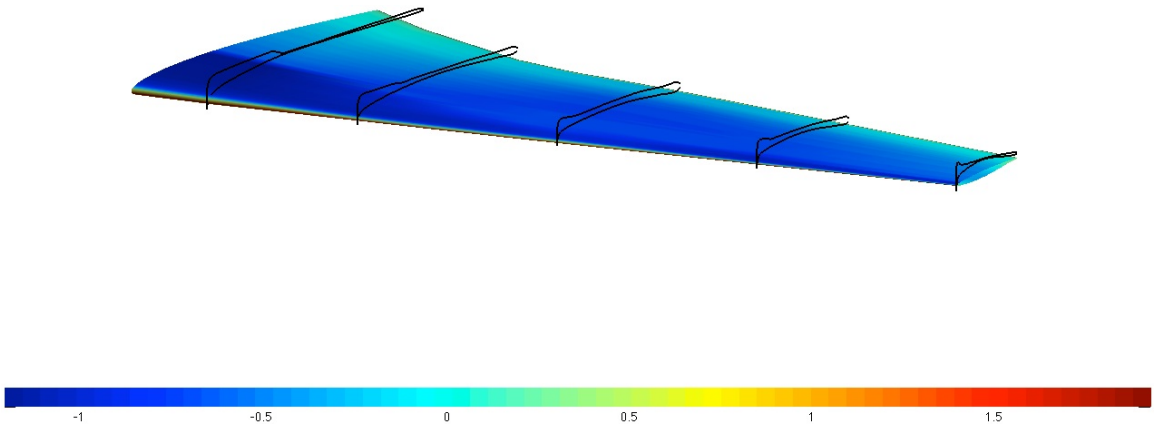

Figure 2. Surface Pressure Distribution of CRM Rigid Wing Model at Mach 0.85 Computed by VORLAX with Transonic and Boundary Layer Corrections

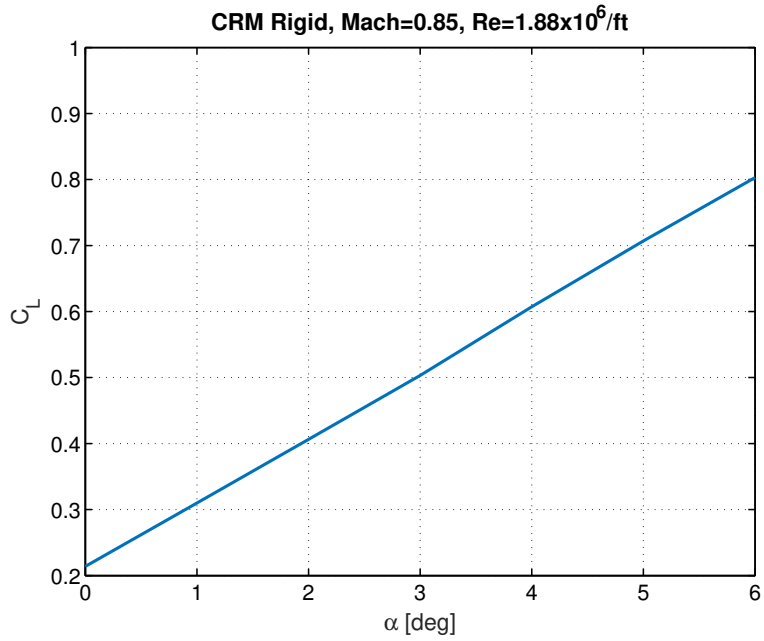

Figure 3. Lift Curve of CRM Rigid Wing Computed by VORLAX with Transonic and Boundary Layer Corrections

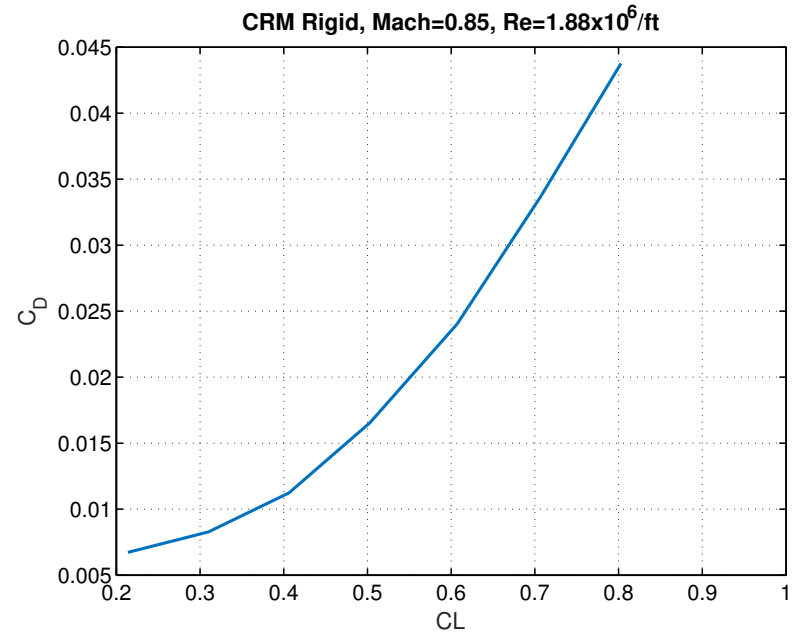

Figure 4. Drag Polar of CRM Rigid Wing Computed by VORLAX with Transonic and Boundary Layer Corrections

The aeroelastic effect on the aerodynamic performance is typically described by the following equation for the local aeroelastic angle of attack defined with respect to the elastic axis according to the linear bending theory:

$$\alpha_c = \frac{\alpha}{\cos\Lambda} - W_x \tan\Lambda - \Theta \tag{1}$$

where x is the coordinate of the elastic axis, α is the wing angle of attack, Λ is the sweep angle of the elastic axis, Θ is the torsional twist (positive nose-down), W is the bending deflection, and the subscript x denotes $\frac{\partial}{\partial x}$.

Thus, the wing bending deflection generally causes a reduction in lift due to the decrease in the local aeroelastic angle of attack for a sweptback wing with $\Lambda > 0$. The torsional twist is generally nose-down (positive in the sign convention). Thus, the net effect is a reduction in lift as well as a change in the design spanwise lift distribution which can affect the induced drag. If the effect of the nonlinear large deflection bending is significant, then clearly this cannot be neglected in the aerodynamic performance analysis of a high aspect ratio flexible wing structure.

III. Nonlinear Large Bending Deflection Analysis

To analyze the nonlinear large deflection bending effect, we perform a strain analysis. Toward that end, consider an airfoil section on the left wing as shown in Fig. 5 undergoing a combined axial, bending, and torsional displacement field. Let (x, y, z) be the undeformed coordinates of point Q on a wing airfoil section in the reference frame D defined by unit vectors $(\mathbf{d}_1, \mathbf{d}_2, \mathbf{d}_3)$. Let $\mathbf{p}_0 = x\mathbf{d}_1$ be a position vector along the elastic axis. Then, point Q is defined by a position vector $\mathbf{p} = \mathbf{p}_0 + \mathbf{q}$ where $\mathbf{q} = y\mathbf{d}_2 + z\mathbf{d}_3$ defines point Q in the $y - z$ plane from the elastic axis. Then, the undeformed local airfoil coordinates of point Q are

$$\begin{bmatrix} y \\ z \end{bmatrix} = \begin{bmatrix} \cos\gamma & -\sin\gamma \\ \sin\gamma & \cos\gamma \end{bmatrix} \begin{bmatrix} \eta \\ \xi \end{bmatrix} \tag{2}$$

where η and ξ are local airfoil coordinates, and γ is the wing section pre-twist angle, positive nose-down.[12,13]

Differentiating y and z with respect to x gives

$$\begin{bmatrix} y_x \\ z_x \end{bmatrix} = \gamma' \begin{bmatrix} -\sin\gamma & -\cos\gamma \\ \cos\gamma & -\sin\gamma \end{bmatrix} \begin{bmatrix} \eta \\ \xi \end{bmatrix} = \begin{bmatrix} -z\gamma' \\ y\gamma' \end{bmatrix} \tag{3}$$

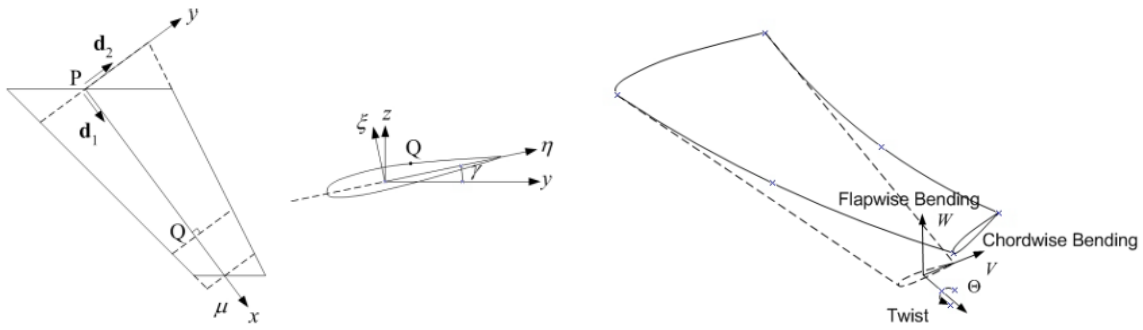

Figure 5. Left Wing Reference Frame of Wing in Combined Bending-Torsion

Let Θ be a torsional twist angle about the x-axis, positive nose-down. Let W and V be flapwise and chordwise bending deflections of point Q, respectively, and W is allowed to be large relative to V. Let U be the axial displacement of point Q. Then, the displacement and rotation vectors due to the elastic deformation can be expressed as

$$\mathbf{r} = U\mathbf{d}_1 + V\mathbf{d}_2 + W\mathbf{d}_3 \tag{4}$$

$$\boldsymbol{\phi} = \Theta\mathbf{d}_1 - \sin^{-1} W_s\mathbf{d}_2 + V_x\mathbf{d}_3 \tag{5}$$

where the subscripts x and s denote the partial derivatives of W and V with respect to x and the arc length s. Note that the term $\sin^{-1} W_s$ represents the rotation angle due to the large flapwise bending with respect to the arc length. If W_s is small, then the usual approximation $\sin^{-1} W_s \approx W_x$ applies. Otherwise, $W_x = W_s s_x$ applies where

$$s_x = \frac{ds}{dx} = \sqrt{1 + y_x^2 + z_x^2} = \sqrt{1 + (y^2 + z^2)(\gamma')^2} \tag{6}$$

Let (x_1, y_1, z_1) be the deformed coordinates of point Q on the airfoil in the reference frame D and $\mathbf{p}_1 = x_1\mathbf{d}_1 + y_1\mathbf{d}_2 + z_1\mathbf{d}_3$ be its position vector. Then the coordinates (x_1, y_1, z_1) are computed as

$$\mathbf{p}_1 = \mathbf{p} + \mathbf{r} + \boldsymbol{\phi} \times \mathbf{q} \tag{7}$$

where

$$\begin{bmatrix} x_1 \\ y_1 \\ z_1 \end{bmatrix} = \begin{bmatrix} x + U - yV_x - z\sin^{-1} W_s \\ y + V - z\Theta \\ z + W + y\Theta \end{bmatrix} \tag{8}$$

Differentiating x_1, y_1, and z_1 with respect to x yields

$$\begin{bmatrix} x_{1,x} \\ y_{1,x} \\ z_{1,x} \end{bmatrix} = \begin{bmatrix} 1 + U_x - yV_{xx} + z\gamma^{'}V_x - z\frac{W_{ss}s_x}{\sqrt{1-W_s^2}} - y\gamma^{'}\sin^{-1} W_x \\ -z\gamma^{'} + V_x - z\Theta_x - y\gamma^{'}\Theta \\ y\gamma^{'} + \sin^{-1} W_x + y\Theta_x - z\gamma^{'}\Theta \end{bmatrix} \tag{9}$$

Note that the term $\frac{W_{ss}}{\sqrt{1-W_s^2}}$ represents the physical curvature of the nonlinear bending with a large deflection. This term is consistent with the nonlinear bending curvature formula by Hodges.[14] Other authors[15,16] have used the curvature formula $\frac{W_{ss}}{(1+W_s^2)^{\frac{3}{2}}}$ based on the elementary calculus which is sometimes mistaken as the physical curvature of a beam as stated by Hodges.[14] The curvature formula $\frac{W_{ss}}{\sqrt{1-W_s^2}}$ can be used in the undeformed coordinates whereas the curvature formula $\frac{W_{ss}}{(1+W_s^2)^{\frac{3}{2}}}$ must be used in the deformed coordinates which are impractical for implementation.

Neglecting the transverse shear effect, the longitudinal strain is computed as[13]

$$\epsilon = \frac{ds_1 - ds}{ds} = \frac{s_{1,x}}{s_x} - 1 \tag{10}$$

where

$$\begin{aligned} s_{1,x} &= \sqrt{x_{1,x}^2 + y_{1,x}^2 + z_{1,x}^2} \\ &= \sqrt{s_x^2 + 2U_x - 2yV_{xx} - 2z\frac{W_{ss}s_x}{\sqrt{1-W_s^2}} + 2\left(y^2+z^2\right)\gamma'\Theta_x + \left(x_{1,x}-1\right)^2 + \left(y_{1,x} + z\gamma'\right)^2 + \left(z_{1,x} - y\gamma'\right)^2} \end{aligned} \tag{11}$$

$s_{1,x}$ is approximated by a Taylor series expansion as

$$s_{1,x} \approx s_x + U_x - yV_{xx} - z\frac{W_{ss}s_x}{\sqrt{1-W_s^2}} + \left(y^2+z^2\right)\gamma^{'}\Theta_x + \frac{\left(x_{1,x}-1\right)^2 + \left(y_{1,x} + z\gamma^{'}\right)^2 + \left(z_{1,x} - y\gamma^{'}\right)^2}{2} + \cdots \tag{12}$$

The slope of the twist angle $\gamma^{'}$ can play a significant role in structures with large twists such as turbomachinery blades. For aircraft wings, this effect is negligible and therefore can be neglected. Thus, for a small wing twist angle slope, $\gamma^{'} \approx 0$ and $s_x \approx 1$. Then $W_s \approx W_x$ and $W_{ss} \approx W_{xx}$. Thus, the longitudinal strain is then obtained as

$$\begin{aligned} \epsilon = U_x - yV_{xx} - z\frac{W_{xx}}{\sqrt{1-W_x^2}} + \frac{1}{2}U_x^2 + \frac{1}{2}V_x^2 + \frac{1}{2}\left(\sin^{-1} W_x\right)^2 + \frac{1}{2}\left(y^2+z^2\right)\Theta_x^2 + \frac{1}{2}y^2V_{xx}^2 \\ + \frac{1}{2}z^2\frac{W_{xx}^2}{1-W_x^2} - yU_xV_{xx} - zU_x\frac{W_{xx}}{\sqrt{1-W_x^2}} + yzV_{xx}\frac{W_{xx}}{\sqrt{1-W_x^2}} - zV_x\Theta_x + y\sin^{-1} W_x\Theta_x \end{aligned} \tag{13}$$

Assuming that the neutral axis of a wing section passes through the elastic axis, then the axial force and moments acting on a wing are evaluated as[8]

$$\begin{aligned} P_x = \int E\epsilon dA = EAU_x + \frac{1}{2}EA\left[U_x^2 + V_x^2 + \left(\sin^{-1} W_x\right)^2\right] + \frac{1}{2}EI_{xx}\Theta_x^2 + \frac{1}{2}EI_{zz}V_{xx}^2 \\ + \frac{1}{2}EI_{yy}\frac{W_{xx}^2}{1-W_x^2} - \left(EAe_aU_x + EI_{yz}\frac{W_{xx}}{\sqrt{1-W_x^2}}\right)V_{xx} \end{aligned} \tag{14}$$

$$M_x = GJ\Theta_x + \int E\epsilon\left(y^2+z^2\right)\Theta_x dA = \left[GJ + EI_{xx}U_x - (1+U_x)\left(EB_3V_{xx} + EB_2\frac{W_{xx}}{\sqrt{1-W_x^2}}\right)\right.$$
$$\left. + \frac{1}{2}EI_{xx}\left[U_x^2 + V_x^2 + \left(\sin^{-1}W_x\right)^2\right] + \frac{1}{2}EB_4V_{xx}^2 + \frac{1}{2}EB_5\frac{W_{xx}^2}{1-W_x^2} + EB_6V_{xx}\frac{W_{xx}}{\sqrt{1-W_x^2}}\right]\Theta_x$$
$$+ \left(-EB_2V_x + EB_3\sin^{-1}W_x\right)\Theta_x^2 + \frac{1}{2}EB_1\Theta_x^3 \quad (15)$$

$$M_y = -\int E\epsilon z dA = (1+U_x)\left(EI_{yy}\frac{W_{xx}}{\sqrt{1-W_x^2}} - EI_{yz}V_{xx}\right) - \frac{1}{2}EB_2\Theta_x^2 - \frac{1}{2}EB_7V_{xx}^2$$
$$- \frac{1}{2}EB_8\frac{W_{xx}^2}{1-W_x^2} - EB_9V_{xx}\frac{W_{xx}}{\sqrt{1-W_x^2}} + \left(EI_{yy}V_x + EI_{yz}\sin^{-1}W_x\right)\Theta_x \quad (16)$$

$$M_z = -\int E\epsilon y dA = (1+U_x)\left(-EI_{yz}\frac{W_{xx}}{\sqrt{1-W_x^2}} + EI_{zz}V_{xx}\right) - \frac{1}{2}EB_3\Theta_x^2 - \frac{1}{2}EB_{10}V_{xx}^2$$
$$- \frac{1}{2}EB_9\frac{W_{xx}^2}{1-W_x^2} - EB_7V_{xx}\frac{W_{xx}}{\sqrt{1-W_x^2}} - \left(EI_{yz}V_x + EI_{zz}\sin^{-1}W_x\right)\Theta_x \quad (17)$$

where E is the Young's modulus, G is the shear modulus, A is the tensile area, J is the torsional constant, and B_i, $i = 1, 2, \ldots, 10$ are defined as

$$\begin{bmatrix} B_1 \\ B_2 \\ B_3 \\ B_4 \\ B_5 \\ B_6 \\ B_7 \\ B_8 \\ B_9 \\ B_{10} \end{bmatrix} = \int \begin{bmatrix} \left(y^2+z^2\right)^2 \\ z\left(y^2+z^2\right) \\ y\left(y^2+z^2\right) \\ y^2\left(y^2+z^2\right) \\ z^2\left(y^2+z^2\right) \\ yz\left(y^2+z^2\right) \\ y^2z \\ z^3 \\ yz^2 \\ y^3 \end{bmatrix} dA \quad (18)$$

For a rectangular wing box structure with the neutral axis in coincidence with the elastic axis, the constants B_1, B_4, and B_5 are generally much larger than the other constants B_i, $i \neq 1, 4, 5$ and can be approximated as

$$\begin{bmatrix} B_1 \\ B_4 \\ B_5 \end{bmatrix} \approx \frac{1}{A}\begin{bmatrix} I_{xx}^2 \\ I_{xx}I_{zz} \\ I_{xx}I_{yy} \end{bmatrix} \quad (19)$$

Assuming that the nonlinear contributions of the chordwise bending deflection are small and neglecting the cross-product inertia I_{yz} and the small constants B_i, $i \neq 1, 4, 5$, then the following simplification can be made:

$$P_x = EAU_x + \frac{1}{2}EA\left[U_x^2 + \left(\sin^{-1}W_x\right)^2\right] + \frac{1}{2}EI_{xx}\Theta_x^2 + \frac{1}{2}EI_{yy}\frac{W_{xx}^2}{1-W_x^2} \quad (20)$$

$$M_x = \left(GJ + P_xr_k^2\right)\Theta_x \quad (21)$$

$$M_y = (1+U_x)\,EI_{yy}\frac{W_{xx}}{\sqrt{1-W_x^2}} \quad (22)$$

$$M_z = EI_{zz}V_{xx} - EI_{zz}\sin^{-1}W_x\Theta_x \quad (23)$$

where $r_k = \sqrt{\frac{I_{xx}}{A}}$ is the radius of gyration.

Note that the signs of the moments are defined in the positive deflection sense such that

$$\mathbf{M} = M_x \mathbf{d}_1 - M_y \mathbf{d}_2 + M_z \mathbf{d}_3 \tag{24}$$

The resulting equilibrium equations are given by[8]

$$\frac{\partial}{\partial x} \begin{bmatrix} P_x \\ P_y \\ P_z \end{bmatrix} = - \begin{bmatrix} f_x \\ f_y \\ f_z \end{bmatrix} \tag{25}$$

$$\frac{\partial}{\partial x} \begin{bmatrix} M_x \\ M_y \\ M_z \end{bmatrix} = \begin{bmatrix} P_y W_x - P_z V_x - m_x \\ P_x W_x - P_z + m_y \\ P_x V_x - P_y - m_z \end{bmatrix} \tag{26}$$

These equations become

$$\frac{\partial M_x}{\partial x} + \underbrace{\left(\frac{\partial M_z}{\partial x} - P_x V_x + m_z \right)}_{0} W_x - \underbrace{\left(\frac{\partial M_y}{\partial x} - P_x W_x - m_y \right)}_{0} V_x + m_x = 0 \tag{27}$$

$$\frac{\partial^2 M_y}{\partial x^2} - \frac{\partial \left(P_x W_x \right)}{\partial x} - \frac{\partial m_y}{\partial x} - f_z = 0 \tag{28}$$

$$\frac{\partial^2 M_z}{\partial x^2} - \frac{\partial \left(P_x V_x \right)}{\partial x} + \frac{\partial m_z}{\partial x} - f_y = 0 \tag{29}$$

The resulting nonlinear equations are obtained as

$$\frac{\partial}{\partial x} \left\{ EAU_x + \frac{1}{2} EA \left[U_x^2 + \left(\sin^{-1} W_x \right)^2 \right] + \frac{1}{2} EI_{xx} \Theta_x^2 + \frac{1}{2} EI_{yy} \frac{W_{xx}^2}{1 - W_x^2} \right\} = -f_x \tag{30}$$

$$\frac{\partial}{\partial x} \left[\left(GJ + P_x r_k^2 \right) \Theta_x \right] = -m_x \tag{31}$$

$$\frac{\partial^2}{\partial x^2} \left[\left(1 + U_x \right) EI_{yy} \frac{W_{xx}}{\sqrt{1 - W_x^2}} \right] - \frac{\partial \left(P_x W_x \right)}{\partial x} = f_z + \frac{\partial m_y}{\partial x} \tag{32}$$

$$\frac{\partial^2}{\partial x^2} \left(EI_{zz} V_{xx} - EI_{zz} \sin^{-1} W_x \Theta_x \right) - \frac{\partial \left(P_x V_x \right)}{\partial x} = f_y - \frac{\partial m_z}{\partial x} \tag{33}$$

IV. Static Aeroelasticity

The forces and moments on the right hand side of Eqs. (30) - (33) include all external and inertial forces and moments due to the acceleration of the wing structure. In order to compute the aerodynamic forces and moments of a flexible wing structure, static aeroelasticity must be considered.

The relative velocity of the air approaching a wing section includes the contributions from the wing aeroelastic deflections that result in changes in the local angle of attack. Since aerodynamic forces and moments are dependent on the local angle of attack, the wing aeroelastic deflections will generate additional elastic forces and moments. The local angle of attack depends on the relative approaching air velocity as well as the rotation angle $\boldsymbol{\phi}$ from Eq. (5). The relative air velocity in turn also depends on the deflection-induced velocity. The velocity at point Q due to the aircraft velocity and angular velocity in the reference frame D is computed as

$$\begin{aligned} \mathbf{v}_Q &= \bar{\mathbf{v}} + \boldsymbol{\omega} \times \mathbf{r} = \left(u\mathbf{b}_1 + v\mathbf{b}_2 + w\mathbf{b}_3 \right) + \left(p\mathbf{b}_1 + q\mathbf{b}_2 + r\mathbf{b}_3 \right) \times \left(-x_a \mathbf{b}_1 - y_a \mathbf{b}_2 - z_a \mathbf{b}_3 \right) \\ &= \left(u + ry_a - qz_a \right) \mathbf{b}_1 + \left(v - rx_a + pz_a \right) \mathbf{b}_2 + \left(w + qx_a - py_a \right) \mathbf{b}_3 \\ &= x_t \mathbf{d}_1 + y_t \mathbf{d}_2 + z_t \mathbf{d}_3 \end{aligned} \tag{34}$$

where $(\mathbf{b}_1, \mathbf{b}_2, \mathbf{b}_3)$ are the unit vectors in the standard aircraft body-fixed reference frame B. The coordinate transformation between the reference frame B and D is given by

$$\begin{bmatrix} \mathbf{b}_1 \\ \mathbf{b}_2 \\ \mathbf{b}_3 \end{bmatrix} = \begin{bmatrix} -\sin\Lambda\cos\Gamma & -\cos\Lambda & \sin\Lambda\sin\Gamma \\ -\cos\Lambda\cos\Gamma & \sin\Lambda & \cos\Lambda\sin\Gamma \\ -\sin\Gamma & 0 & -\cos\Gamma \end{bmatrix} \begin{bmatrix} \mathbf{d}_1 \\ \mathbf{d}_2 \\ \mathbf{d}_3 \end{bmatrix} \tag{35}$$

where Γ is the wing dihedral angle.

(x_t, y_t, z_t) are the velocity components in the left wing coordinate reference frame D and are computed as

$$\begin{bmatrix} x_t \\ y_t \\ z_t \end{bmatrix} = \begin{bmatrix} -(u + ry_a - qz_a)\sin\Lambda\cos\Gamma - (v - rx_a + pz_a)\cos\Lambda\cos\Gamma - (w + qx_a - py_a)\sin\Gamma \\ -(u + ry_a - qz_a)\cos\Lambda + (v - rx_a + pz_a)\sin\Lambda \\ (u + ry_a - qz_a)\sin\Lambda\sin\Gamma + (v - rx_a + pz_a)\cos\Lambda\sin\Gamma - (w + qx_a - py_a)\cos\Gamma \end{bmatrix} \tag{36}$$

where (u, v, w) are the aircraft velocity components, (p, q, r) are aircraft angular velocity components in the roll, pitch, and yaw axes, and (x_a, y_a, z_a) is the coordinate of point Q in the aircraft body-fixed reference frame B relative to the aircraft CG (center of gravity) such that x_a is positive when point Q is aft of the aircraft CG, y_a is positive when point Q is toward the left wing from the aircraft CG, and z_a is positive when point Q is above the aircraft CG.

Consider a trim problem when $\beta = 0$, $p = q = r = 0$ for steady-state aerodynamics. For simplicity, we assume $\Gamma = 0$. Then,

$$\begin{bmatrix} x_t \\ y_t \\ z_t \end{bmatrix} = \begin{bmatrix} -u\sin\Lambda \\ -u\cos\Lambda \\ -w \end{bmatrix} \tag{37}$$

The velocity must be transformed from the reference frame D to the airfoil local coordinate reference frame defined by (μ, η, ξ) as follows:

$$\begin{bmatrix} v_\mu \\ v_\eta \\ v_\xi \end{bmatrix} = \begin{bmatrix} 1 & 0 & 0 \\ 0 & \cos\Theta & \sin\Theta \\ 0 & -\sin\Theta & \cos\Theta \end{bmatrix} \begin{bmatrix} \cos V_x & \sin V_x & 0 \\ -\sin V_x & \cos V_x & 0 \\ 0 & 0 & 1 \end{bmatrix} \times \times \begin{bmatrix} \cos\left(\sin^{-1} W_x\right) & 0 & \sin\left(\sin^{-1} W_x\right) \\ 0 & 1 & 0 \\ -\sin\left(\sin^{-1} W_x\right) & 0 & \cos\left(\sin^{-1} W_x\right) \end{bmatrix} \begin{bmatrix} x_t \\ y_t \\ z_t \end{bmatrix} \tag{38}$$

Making the small angle assumption for Θ and V_x only and neglecting the nonlinear terms that contain V_x, then the velocity components in the local coordinate reference frame are computed as

$$\begin{bmatrix} v_\mu \\ v_\eta \\ v_\xi \end{bmatrix} = \begin{bmatrix} x_t\sqrt{1 - W_x^2} + y_t V_x + z_t W_x \\ -x_t\left(V_x + \Theta W_x\right) + y_t + z_t\Theta\sqrt{1 - W_x^2} \\ -x_t W_x - y_t\Theta + z_t\sqrt{1 - W_x^2} \end{bmatrix} \tag{39}$$

For a small angle of attack, the usual assumption of $\alpha = \frac{w}{u}$ is valid, but if the rotation angle due to the flapwise bending is large, then some accuracy in the small angle of attack assumption may be suffered. Therefore, the exact angle of attack definition $\alpha = \tan^{-1}\frac{w}{u}$ is used. Then, the local aeroelastic angle of attack on the airfoil section due to the velocity components v_η and v_ξ defined with respect to the elastic axis is computed as

$$\alpha_c = \tan^{-1}\frac{v_\xi}{v_\eta} \approx \tan^{-1}\frac{\bar{v}_\xi}{\bar{v}_\eta} + \frac{\frac{\Delta v_\xi}{\bar{v}_\eta} - \frac{\bar{v}_\xi \Delta v_\eta}{\bar{v}_\eta^2}}{1 + \left(\frac{\bar{v}_\xi}{\bar{v}_\eta}\right)^2} \tag{40}$$

where

$$\bar{v}_\xi = -w \tag{41}$$

$$\Delta v_\xi = u\sin\Lambda W_x + u\cos\Lambda\Theta - w\left(\sqrt{1 - W_x^2} - 1\right) \tag{42}$$

$$\bar{v}_\eta = -u\cos\Lambda \tag{43}$$

$$\Delta v_\eta = u\sin\Lambda\left(V_x + \Theta W_x\right) - w\Theta\sqrt{1-W_x^2} \tag{44}$$

Then,

$$\alpha_c = \tan^{-1}\left(\frac{w}{u\cos\Lambda}\right) - \frac{1}{1+\frac{w^2}{u^2\cos^2\Lambda}}\frac{u\sin\Lambda W_x + u\cos\Lambda\Theta - w\left(\sqrt{1-W_x^2}-1\right)}{u\cos\Lambda} - \frac{1}{1+\frac{w^2}{u^2\cos^2\Lambda}}\frac{-uw\sin\Lambda\left(V_x+\Theta W_x\right) + w^2\Theta\sqrt{1-W_x^2}}{u^2\cos^2\Lambda} \tag{45}$$

Using the Taylor series approximation of $\sqrt{1-W_x^2} \approx 1 - \frac{W_x^2}{2}$ and upon simplification, we get

$$\alpha_c = \tan^{-1}\left(\frac{\tan\alpha}{\cos\Lambda}\right) - \frac{\cos^2\Lambda}{\cos^2\Lambda+\tan^2\alpha}\frac{\sin\Lambda W_x + \cos\Lambda\Theta + \frac{\tan\alpha W_x^2}{2}}{\cos\Lambda} - \frac{\cos^2\Lambda}{\cos^2\Lambda+\tan^2\alpha}\frac{-\tan\alpha\sin\Lambda\left(V_x+\Theta W_x\right) + \tan^2\alpha\Theta\left(1-\frac{W_x^2}{2}\right)}{\cos^2\Lambda} \tag{46}$$

Using the Taylor series approximation of $\tan^{-1}\left(\frac{\tan\alpha}{\cos\Lambda}\right) \approx \frac{\tan\alpha}{\cos\Lambda}\left(1-\frac{\tan^2\alpha}{6\cos^2\Lambda}\right) \approx \frac{\alpha}{\cos\Lambda}\left(1+\frac{\alpha^2}{6}\right) \times \cdots \left[1-\frac{\alpha^2}{6\cos^2\Lambda}\left(1+\frac{\alpha^2}{6}\right)^2\right] \approx \frac{\alpha}{\cos\Lambda}\left(1-\frac{\alpha^2}{6}\tan^2\Lambda\right)$, the local aeroelastic angle of attack can be expressed as

$$\alpha_c = \alpha_r + \alpha_e \tag{47}$$

where

$$\alpha_r = \frac{\alpha}{\cos\Lambda}\left(1-\frac{\alpha^2\tan^2\Lambda}{6}\right) \tag{48}$$

is the rigid angle of attack due to the aircraft velocity and

$$\alpha_e = \frac{\tan\alpha\sin\Lambda V_x}{\cos^2\Lambda+\tan^2\alpha} - \frac{\cos\Lambda-\tan\alpha\Theta}{\cos^2\Lambda+\tan^2\alpha}\left(\sin\Lambda W_x + \frac{\tan\alpha W_x^2}{2}\right) - \Theta \tag{49}$$

is the elastic angle of attack due to the aeroelastic deflections. Note that the rigid angle of attack is defined with respect to the elastic axis, hence the term $\cos\Lambda$ in the denominator. For a sweptback wing, the contribution of W_x is negative, thus effectively reduces the local angle of attack. The bending deflection thus creates an effective wash-out twist to reduce the local angle of attack for sweptback wings. Consequently, the trim angle of attack must be increased in order to compensate for the wash-out twist. Equation (49) for nonlinear large deflection bending should be contrasted with Eq. (1) for linear small deflection bending.

A. Forces and Moments

The aerodynamic and body forces and moments are given by

$$\begin{bmatrix} f_x \\ f_y \\ f_z \\ m_x \\ m_y \\ m_z \end{bmatrix} = \begin{bmatrix} c_D q_\infty c\sin\Lambda\cos\Lambda \\ c_D q_\infty c\cos^2\Lambda \\ c_L q_\infty c\cos\Lambda - mg \\ -c_m q_\infty c^2\cos^2\Lambda + mge_{cg} \\ c_m q_\infty c^2\sin\Lambda\cos\Lambda \\ 0 \end{bmatrix} \tag{50}$$

where q_∞ is the dynamic pressure, c is the chord length, m is the mass distribution, g is the gravity acceleration, and e_{cg} is the offset of the center of mass from the elastic axis (positive with the center of mass aft of the elastic axis).

The steady-state lift, drag, and pitching moment coefficients in the streamwise direction can be generally modeled as

$$c_L = c_{L_0} + c_{L_\alpha}(\alpha)\,\alpha_c \cos\Lambda \tag{51}$$

$$c_D = c_{D_0} + c_{D_\alpha}(\alpha)\,\alpha_c \cos\Lambda + c_{D^2_\alpha}(\alpha)\,\alpha_c^2 \cos^2\Lambda \tag{52}$$

$$c_m = c_{m_{ac}}(\alpha) + c_L \frac{e}{c} \tag{53}$$

where c_{L_0} and c_{D_0} are the lift and drag coefficients at zero angle of attack, c_{L_α} is the lift curve slope, c_{D_α} and $c_{D_{\alpha^2}}$ are the drag derivatives with respect to the angle of attack, $c_{m_{ac}}$ is the pitching moment coefficient at the aerodynamic center, and e is the offset of the aerodynamic center from the elastic axis, positive with the aerodynamic center forward of the elastic axis. The nonlinear effect of large angles of attack in the aerodynamic coefficients is reflected in the general functions $c_{L_\alpha}(\alpha)$, $c_{D_\alpha}(\alpha)$, $c_{D_{\alpha^2}}(\alpha)$, and $c_{m_{ac}}(\alpha)$. These functions take on constant values for small angles of attack below stall.

B. Effect of Nonlinear Bending Theory on Lifting Line Aerodynamics

Consider the case of unswept wings, then $f_x = 0$. The local angle of attack is reduced to

$$\alpha_c = \alpha - \frac{1 - \tan\alpha\Theta}{1 + \tan^2\alpha} \frac{\tan\alpha W_x^2}{2} - \Theta \tag{54}$$

For linear structures, the wing bending deflection has no effect on the wash-out twist for unswept wings. In contrast, for nonlinear structures, the contribution of the wing bending deflection to the wash-out twist is non-zero due to the term W_x^2, although this term is small. Nonetheless, this results in a bending-torsion aeroelastic coupling even though the wings are unswept. This coupling does not exist in linear bending theory. This term can significantly affect the lift distribution and the induced drag of a high aspect ratio flexible wing as will be shown.

Since there is no applied axial force at the end of the cantilever wing, the axial displacement equation is equal to zero

$$P_x = EAU_x + \frac{1}{2}EA\left[U_x^2 + \left(\sin^{-1} W_x\right)^2\right] + \frac{1}{2}EI_{xx}\Theta_x^2 + \frac{1}{2}EI_{yy}\frac{W_{xx}^2}{1 - W_x^2} = 0 \tag{55}$$

Solving for U_x from Eq. (55) yields

$$1 + U_x = \sqrt{1 - \left(\sin^{-1} W_x\right)^2 - \frac{I_{xx}}{A}\Theta_x^2 - \frac{I_{yy}}{A}\frac{W_{xx}^2}{1 - W_x^2}} \tag{56}$$

Then, the nonlinear static aeroelastic equations become

$$\frac{\partial}{\partial x}\left(GJ\Theta_x\right) + c_{L_\alpha} q_\infty e c \left(\frac{1 - \tan\alpha\Theta}{1 + \tan^2\alpha}\frac{\tan\alpha W_x^2}{2} + \Theta\right) = c_{m_r} q_\infty c^2 - mge_{cg} \tag{57}$$

$$\frac{\partial^2}{\partial x^2}\left[EI_{yy}W_{xx}\sqrt{\frac{1 - \left(\sin^{-1} W_x\right)^2 - r_k^2\Theta_x^2 - \frac{I_{yy}}{A}\frac{W_{xx}^2}{1 - W_x^2}}{1 - W_x^2}}\right] + c_{L_\alpha} q_\infty c \left(\frac{1 - \tan\alpha\Theta}{1 + \tan^2\alpha}\frac{\tan\alpha W_x^2}{2} + \Theta\right) = c_{L_r} q_\infty c - mg \tag{58}$$

$$\frac{\partial^2}{\partial x^2}\left(EI_{zz}V_{xx} - EI_{zz}\sin^{-1} W_x \Theta_x\right) + \left(c_{D_\alpha} + 2c_{D^2_\alpha}\alpha\right) q_\infty c \left(\frac{1 - \tan\alpha\Theta}{1 + \tan^2\alpha}\frac{\tan\alpha W_x^2}{2} + \Theta\right) - c_{D^2_\alpha} q_\infty c \left(\frac{1 - \tan\alpha\Theta}{1 + \tan^2\alpha}\frac{\tan\alpha W_x^2}{2} - \Theta\right)^2 = c_{D_r} q_\infty c \tag{59}$$

where $c_{L_r} = c_{L_0} + c_{L_\alpha}\alpha$ is the rigid lift coefficient, $c_{D_r} = c_{D_0} + c_{D_\alpha}\alpha + c_{D_{\alpha^2}}\alpha^2$ is the rigid drag coefficient, and $c_{m_r} = c_{m_{ac}} + c_{L_r}\frac{e}{c}$ is the rigid pitching moment coefficient about the elastic axis.

If the torsional twist is small relative to the flapwise bending slope, then the nonlinear static aeroelastic equation for bending is expressed as

$$\frac{\partial^2}{\partial x^2}\left[EI_{yy}W_{xx}\sqrt{\frac{1-\left(\sin^{-1}W_x\right)^2-\frac{I_{yy}}{A}\frac{W_{xx}^2}{1-W_x^2}}{1-W_x^2}}\right]+c_{L_\alpha}q_\infty c\frac{\tan\alpha W_x^2}{2\left(1+\tan^2\alpha\right)}=c_{L_r}q_\infty c-mg \tag{60}$$

For the nonlinear large deflection bending of the wing structure, a modified lifting line theory is used. The velocity induced by a trailing vortex at $x=x_0$ acting at the quarter chord is given by the Biot-Savart law according to[17]

$$d\mathbf{v}_i=\frac{\mathbf{r}\times\mathbf{V}}{4\pi V_\infty\mathbf{r}.\mathbf{r}}\frac{d\Gamma}{ds}ds \tag{61}$$

where $\frac{d\Gamma}{ds}$ is the lift circulation distribution along the arc length s of the wing, $\mathbf{r}=-\left(x_0-x+U_0-U\right)\mathbf{d}_1-\left(W_0-e\Theta_0-W+e\Theta\right)\mathbf{d}_3$, and $\mathbf{V}=V_\infty\mathbf{d}_2$. This yields the following expression:

$$d\mathbf{v}_i=\frac{-\left(x_0-x+U_0-U\right)\mathbf{d}_3+\left(W_0-e\Theta_0-W+e\Theta\right)\mathbf{d}_1}{4\pi\mathbf{r}.\mathbf{r}}\frac{d\Gamma}{ds}ds \tag{62}$$

Due to the axial displacement and flapwise bending effects, in addition to the induced downwash velocity component, there also exists an induced sidewash velocity component. The effective downwash along the arc length of the wing is the induced velocity component normal to the vortex sheet.[17] This is given by

$$dw_i=d\mathbf{v}_i.\mathbf{n}_0 \tag{63}$$

where $\mathbf{n}_0=\left[W_{x,0}\mathbf{d}_1-\left(1+U_{x,0}\right)\mathbf{d}_3\right]\frac{dx_0}{ds_0}$ and $ds_0=dx_0\sqrt{\left(1+U_{x,0}\right)^2+W_{x,0}^2}$. Then,

$$dw_i=\frac{\left(x_0-x+U_0-U\right)\left(1+U_{x,0}\right)+\left(W_0-e\Theta_0-W+e\Theta\right)W_{x,0}}{4\pi\left[\left(x_0-x+U_0-U\right)^2+\left(W_0-e\Theta_0-W+e\Theta\right)^2\right]}\frac{dx_0}{ds_0}\frac{d\Gamma}{ds}ds \tag{64}$$

where Θ_0, U_0, $U_{x,0}$ W_0, and $W_{x,0}$ are the wing torsional twist, axial displacement, axial displacement derivative, bending deflection, and bending slope, respectively, at $x=x_0$.

The total induced downwash at $x=x_0$ is then evaluated by the following expression:

$$w_i\left(x_0\right)=-\int_{-\frac{b}{2}}^{\frac{b}{2}}\frac{\left(x_0-x+U_0-U\right)\left(1+U_{x,0}\right)+\left(W_0-e\Theta_0-W+e\Theta\right)W_{x,0}}{4\pi\left[\left(x_0-x+U_0-U\right)^2+\left(W_0-e\Theta_0-W+e\Theta\right)^2\right]}\frac{dx_0}{ds_0}\frac{d\Gamma}{dx}dx \tag{65}$$

Note that if $U=0$ and $U_x=0$, Eq. (65) recovers the downwash expression given by Cones.[17]

The general lift circulation distribution is expressed as

$$\Gamma=\Gamma_r+\Gamma_e \tag{66}$$

where Γ_r and Γ_e are the rigid and aeroelastic components of the lift circulation distribution which are given by

$$\Gamma_r=\frac{1}{2}V_\infty cc_{L_r} \tag{67}$$

$$\Gamma_e=\frac{1}{2}V_\infty cc_{L_\alpha}\left(-\frac{1-\tan\alpha\Theta}{1+\tan^2\alpha}\frac{\tan\alpha W_x^2}{2}-\Theta\right) \tag{68}$$

Thus, the induced angle of attack is not only a function of the lift distribution but also is a function of the axial displacement, bending deflection, and torsional twist.

Consider a special case of the ideal elliptical lift distribution for a rigid wing $\Gamma_r=\Gamma_0\sqrt{1-\left(\frac{2x'}{b+2U_t}\right)^2}$ where $x'=x+U$ is the coordinate of the elastic axis for the deformed wing and $U_t=U\left(\frac{b}{2}\right)$. We use the coordinate of the deformed wing to specify lift distribution to ensure that the solution is physical. Otherwise,

the lift circulation at $x^{'} = \pm\frac{b}{2}$ does not exist since $x^{'} \in \left[-\frac{b}{2} - U_t, \frac{b}{2} + U_t\right]$. Then, the downwash expression becomes

$$w_i\left(x_0\right) = -\int_{-\frac{b}{2}-U_t}^{\frac{b}{2}+U_t} \frac{\left(x_0^{'} - x^{'}\right)\left(1 + U_{x,0}\right) + \left(W_0 - e\Theta_0 - W + e\Theta\right) W_{x,0}}{4\pi\left[\left(x_0^{'} - x^{'}\right)^2 + \left(W_0 - e\Theta_0 - W + e\Theta\right)^2\right]} \frac{dx_0}{ds_0} \times \left[-\frac{4\Gamma_0 x^{'}}{b^2\sqrt{1 - \left(\frac{2x^{'}}{b+2U_t}\right)^2}} + \frac{d\Gamma_e}{dx^{'}}\right] dx^{'} \quad (69)$$

For a rigid wing, the ideal elliptical lift distribution produces a uniform induced downwash and the minimum induced drag. The effect of the wing bending is to alter this uniform downwash for the ideal elliptical lift distribution. As a result, the ideal elliptical lift distribution design for a rigid wing will not yield the minimum induced drag due to the nonlinear large bending deflection. Wing twist is normally used to change the lift distribution design for a flexible wing.

As an example, consider a constant-section high aspect ratio wing with 1-ft chord and 30-ft span. The cross section is a NACA 0012 with a wall thickness of 0.25 inches and a modulus of elasticity of 10×10^6 psi for aluminum. The cross sectional area and the flapwise area moment of inertia are computed to be $A = 2k_A c t_w$ and $I = \frac{4}{15} k_I c^3 t_w \left(\frac{t}{c}\right)^2$ where $k_A = 1.02084$ and $k_I = 1.03716$. Without considering the nonlinear large deflection effect, the wing is designed for an elliptical lift distribution $l = 100\sqrt{1 - \left(\frac{2x}{b}\right)^2}$ lb/ft where $l = \rho_\infty V_\infty \Gamma$ for $\rho_\infty = 2.37756 \times 10^{-3}$ slug/ft^3 and $V_\infty = 300$ ft/sec corresponding to $M_\infty = 0.2687$. The lift curve slope is estimated from the formula $C_{L_\alpha} = \frac{2\pi}{\sqrt{1 - M_\infty^2} + \frac{2}{\pi AR}}$ where $AR = 30$ is the aspect ratio. This yields $\alpha = 6.89°$. Figure 6 shows the linear and nonlinear deflections of the wing computed by applying the Galerkin method with 10 mode shapes to Eq. (60). Both the wing tip bending deflections as predicted by the linear and nonlinear bending theories are in close agreement The nonlinear bending theory yields a wing tip deflection of 3.0807 ft or 20.54% of the wing semi-span. In comparison, the linear bending theory predicts a wing tip deflection of 3.2137 ft or 21.42% of the wing semi-span. Thus, the nonlinear bending theory predicts a smaller bending deflection than the linear bending theory. This difference is due primarily to the aeroelastic contribution of the last term in the left hand side of Eq. (60).

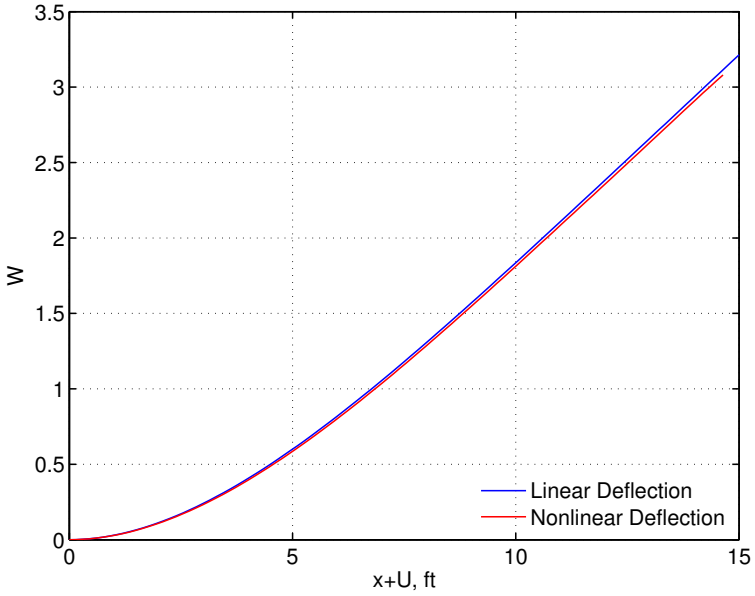

Figure 6. Linear and Nonlinear Bending Deflections

The significant difference between the linear and nonlinear bending theories is the axial displacement. For the linear bending theory, the axial displacement is exactly zero since there is no applied axial force. On the other hand, the nonlinear bending theory predicts an axial displacement of -0.3584 ft or -2.39% of the wing semi-span. As a result, the linear bending theory actually predicts an increase in the wing length by 2.55% of the wing semi-span, whereas the nonlinear bending theory preserves the length of the wing. This length-preserving property of the nonlinear bending theory in effect causes a reduction in the wing aspect ratio, which leads to an increase in the induced drag and decrease in lift as compared to the linear bending theory.

The length-preserving property of the nonlinear bending theory can be shown by examining Eq. (56) and ignoring the terms Θ_x^2 and W_{xx}^2. This leads to

$$U_x = \sqrt{1 - \left(\sin^{-1} W_x\right)^2} - 1 \approx -\frac{1}{2}\left(\sin^{-1} W_x\right)^2 \approx -\frac{1}{2} W_x^2 \tag{70}$$

Thus, it can be seen that U_x is highly dependent on W_x. As the bending deflection increases, the axial displacement decreases.

The change in length due to the nonlinear bending theory is computed as

$$\frac{ds}{dx} = \sqrt{\left(1 + U_x\right)^2 + W_x^2} = \sqrt{1 + \frac{W_x^4}{4}} \approx 1 \tag{71}$$

which shows the length-preserving property of the nonlinear bending theory.

For the linear bending theory, the length is not preserved. Therefore, the increase in length is computed as

$$\Delta L = \int_0^L \left(\sqrt{1 + W_x^2} - 1\right) dx \approx \frac{1}{2}\int_0^L W_x^2 dx \tag{72}$$

This implies that the linear bending theory yields a non-physical solution.

Also ignoring the term W_{xx}^2 in Eq. (60), the nonlinear static aeroelastic equation for bending can be approximated by the Taylor series of $\sin^{-1} W_x \approx W_x\left(1 + \frac{W_x^2}{6}\right)$. Then, the resulting equation is expressed as

$$\frac{\partial^2}{\partial x^2}\left[EI_{yy} W_{xx}\left(1 + \frac{W_x^4}{6}\right)\right] + c_{L_\alpha} q_\infty c \frac{\tan\alpha W_x^2}{2\left(1 + \tan^2\alpha\right)} = c_{L_r} q_\infty c - mg \tag{73}$$

Recognizing that $W_x^4 \approx 0$, then Eq. (73) becomes

$$\frac{\partial^2}{\partial x^2}\left(EI_{yy} W_{xx}\right) + c_{L_\alpha} q_\infty c \frac{\tan\alpha W_x^2}{2\left(1 + \tan^2\alpha\right)} = c_{L_r} q_\infty c - mg \tag{74}$$

Thus, the difference in the bending deflection between the linear and nonlinear bending theories is due to mostly the aeroelastic term in the left hand side which contributes positively to the wing stiffness. For sweptback wings, truss-braced wings,[18] and rotary wings, the effect of the axial tension P_x can be a dominant factor. Then, the significance of the nonlinear large deflection bending can be much more pronounced.

Figure 7 is the effective nonlinear elastic angle of attack due to the term W_x^2 in Eq. (54). This shows that the nonlinear large deflection bending causes a negative angle of attack of about $-0.24°$. This results in a non-elliptical lift distribution as shown in Fig. 8 which is compared to the ideal elliptical lift distribution for the rigid wing and for the flexible wing using the linear bending theory. To illustrate the effect of length-preserving property of the nonlinear bending theory, the lift distribution for the nonlinear large deflection bending is plotted against the displaced coordinate. To restore the ideal elliptical lift distribution, the wing would have to be re-twisted along the wing span to zero out the effect of the elastic angle of attack. Figure 8 shows the elliptical lift distribution plotted in the displaced coordinate.

Figure 9 is the plot of the induced angle of attack $\alpha_i = \frac{w_i}{V_\infty}$ due to the induced downwash over the wing as computed by Eq. (69) which, for the constant chord and negligible torsional twist, is expressed as

$$w_i\left(x_0\right) = -\int_{-\frac{b}{2}-U_t}^{\frac{b}{2}+U_t} \frac{\left(x_0' - x'\right)\left(1 + U_{x,0}\right) + \left(W_0 - e\Theta_0 - W + e\Theta\right) W_{x,0}}{4\pi\left[\left(x_0' - x'\right)^2 + \left(W_0 - e\Theta_0 - W + e\Theta\right)^2\right]} \left[-\frac{4\Gamma_0 x'}{b^2\sqrt{1 - \left(\frac{2x'}{b + 2U_t}\right)^2}} + \frac{d\Gamma_e}{dx'}\right] dx' \tag{75}$$

which takes advantage of the length-preserving property of the nonlinear bending theory.

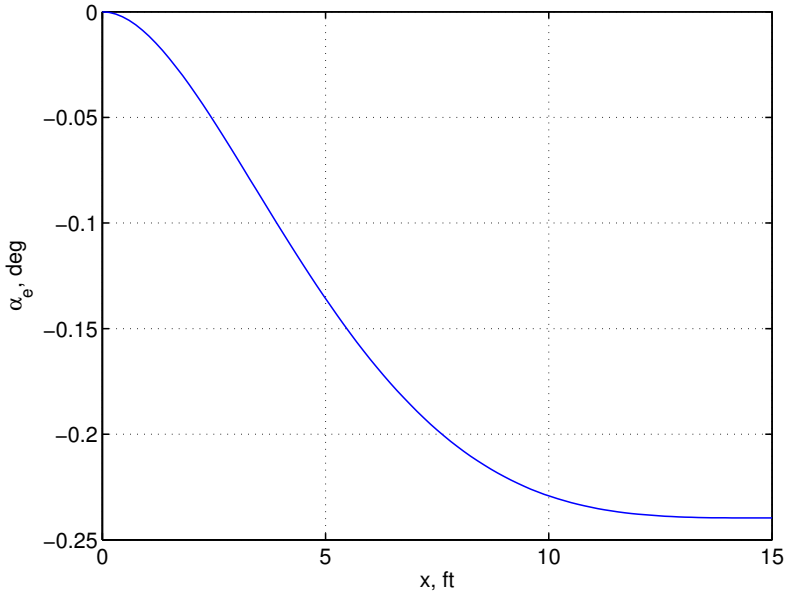

Figure 7. Aeroelastic Angle of Attack due to Nonlinear Bending Deflection

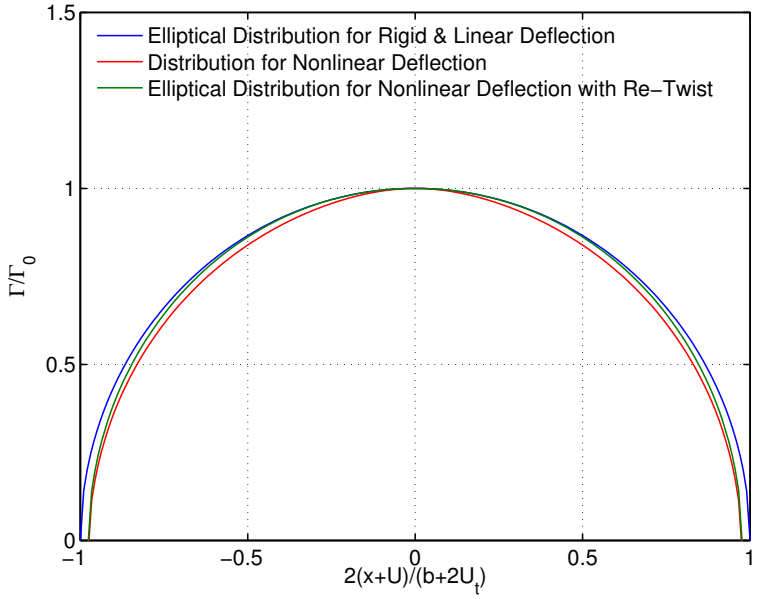

Figure 8. Lift Distributions for Bending Deflections

Note that for the linear bending theory, $\Gamma_e = 0$ and $U = 0$. So, the induced downwash is computed from

the following equation:

$$w_i(x_0) = \int_{-\frac{b}{2}}^{\frac{b}{2}} \frac{(x_0 - x) + (W_0 - e\Theta_0 - W + e\Theta) W_{x,0}}{\pi \left[(x_0 - x)^2 + (W_0 - e\Theta_0 - W + e\Theta)^2 \right]} \frac{1}{\sqrt{1 + W_{x,0}^2}} \frac{\Gamma_0 x}{b^2 \sqrt{1 - \left(\frac{2x}{b}\right)^2}} dx \tag{76}$$

The rigid wing has a constant induced angle of attack for the ideal elliptical lift distribution whereas the bending deflection causes the induced angle of attack to become non-uniform with the maximum value at the mid-wing span. The linear bending theory results in a lower induced angle of attack than the nonlinear deflection. This is due to the difference in the wing span where for the nonlinear deflection there is a reduction in the wing span which causes an increase in the induced downwash, hence induced angle of attack. The induced angle of attack at the center of the wing is the greatest with the nonlinear deflection. The results illustrate the significance of the effect of the nonlinear bending theory on the induced drag of a wing structure. Also shown in Fig. 9 is the induced angle of attack for the nonlinear deflection when the wing is re-twisted to remove the effect of the nonlinear elastic angle of attack. This has an effect of lowering the maximum induced angle of attack for the nonlinear deflection.

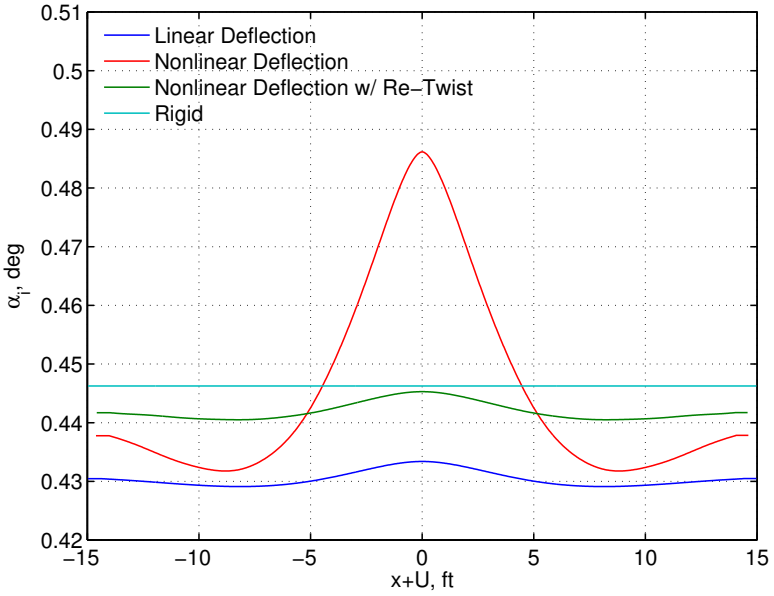

Figure 9. Induced Angles of Attack due to Bending Deflections

The lift coefficient is evaluated by taking into account the wing bending deflection slope and the shortening of the wing span due to the axial displacement according to

$$C_L = \frac{1}{q_\infty S} \int_{-\frac{b}{2}}^{\frac{b}{2}} \rho_\infty V_\infty \Gamma \cos\left(\sin^{-1} W_x\right)(1 + U_x)\, dx = \frac{1}{q_\infty S} \int_{-\frac{b}{2} - U_t}^{\frac{b}{2} + U_t} \rho_\infty V_\infty \Gamma \sqrt{1 - W_x^2}\, dx' \tag{77}$$

The induced drag coefficient is evaluated from the following equation:

$$C_{D_i} = \frac{1}{q_\infty S} \int_{-\frac{b}{2} - U_t}^{\frac{b}{2} + U_t} \rho_\infty V_\infty \Gamma \alpha_i\, dx' \tag{78}$$

Table 1 shows the lift and induced drag coefficients and the span efficiency factors ϵ based on the aspect ratio of the rigid wing for the linear deflection, nonlinear deflection, and rigid wing. The lift and induced drag coefficients are evaluated with the reduced wing span by $2U_t$ for the nonlinear deflection. It can be seen that

the effect of the nonlinear deflection is to reduce both the lift coefficient and the span efficiency. The linear bending theory predicts only a 2.34% lift reduction and 1.19% decrease in the span efficiency relative to the rigid wing. In comparison to the rigid wing, the nonlinear bending theory predicts a 6.69% lift reduction and 9.02% decrease in the span efficiency. Even with re-twisting, the lift reduction only decreases to 4.88%. Thus, the linear bending theory tends to yield more optimistic aerodynamic performance characteristics for a high aspect ratio flexible wing.

	C_L	C_{D_i}	ϵ
Linear Deflection	0.7166	0.005514	0.9881
Nonlinear Deflection	0.6847	0.005468	0.9098
Nonlinear Deflection with Re-Twist	0.6980	0.005515	0.9375
Rigid Wing	0.7338	0.005716	1

Table 1. Lift and Drag Coefficients and Span Efficiency Factors

V. Weak-Form Numerical Solution

The nonlinear partial differential equations are usually referred to as a strong form. A numerical solution can be performed by converting the strong-form partial differential equations into weak-form integral equations by letting $U(x,t) = \mathbf{N}_u(x)\,\mathbf{u}(t)$, $V(x,t) = \mathbf{N}_v(x)\,\mathbf{v}(t)$, $W(x,t) = \mathbf{N}_w(x)\,\mathbf{w}(t)$, and $\Theta(x,t) = \mathbf{N}_\theta(x)\,\boldsymbol{\theta}(t)$. For the Galerkin method, $\mathbf{N}_u(x)$, $\mathbf{N}_v(x)$, $\mathbf{N}_w(x)$, and$\mathbf{N}_\theta(x)$ are the vectors of the mode shapes over the domain of the solution $x \in [0, L]$, whereas for the finite element method they are the vectors of interpolation functions over the domain of the solution for an element $x \in [0, l]$. The vectors $\mathbf{u}(t)$, $\mathbf{v}(t)$, $\mathbf{w}(t)$, and $\boldsymbol{\theta}(t)$ represent the generalized coordinates in the Galerkin method, or the nodal displacements including the bending slopes in the finite element method.

The term $\sin^{-1} W_x$ can be approximated by the first two terms of the Taylor series expansion $W_x\left(1+\frac{W_x^2}{6}\right)$. Pre-multiplying Eqs. (30) to (33) by $\mathbf{N}_u^\top(x)$, $\mathbf{N}_v^\top(x)$, $\mathbf{N}_w^\top(x)$, and $\mathbf{N}_\theta^\top(x)$, respectively, and integrating over the domain of the solution yields

$$-\int \mathbf{N}_u^{'\top} EA\left(1+\frac{1}{2}U_x\right)\mathbf{N}_u^{'}\mathbf{u}dx - \frac{1}{2}\int \mathbf{N}_u^{'\top}\left[EAW_x\left(1+\frac{W_x^2}{6}\right)^2\mathbf{N}_w^{'} + EI_{yy}\frac{W_{xx}}{1-W_x^2}\mathbf{N}_w^{''}\right]\mathbf{w}dx$$
$$-\frac{1}{2}\int \mathbf{N}_u^{'\top} EI_{xx}\Theta_x\mathbf{N}_\theta^{'}\boldsymbol{\theta}dx = -\int \mathbf{N}_u^\top f_x dx \quad (79)$$

$$-\int \mathbf{N}_\theta^{'\top}\left(GJ + P_x r_k^2\right)\mathbf{N}_\theta^{'}\boldsymbol{\theta}dx = -\int \mathbf{N}_\theta^\top m_x dx \quad (80)$$

$$\int\left(\mathbf{N}_w^{''\top} EI_{yy}\frac{1+U_x}{\sqrt{1-W_x^2}}\mathbf{N}_w^{''} + \mathbf{N}_w^{'\top}P_x\mathbf{N}_w^{'}\right)\mathbf{w}dx = \int \mathbf{N}_w^\top\left(f_z + \frac{\partial m_y}{\partial x}\right)dx \quad (81)$$

$$\int\left(\mathbf{N}_v^{''\top} EI_{zz}\mathbf{N}_v^{''} + \mathbf{N}_v^{'\top}P_x\mathbf{N}_v^{'}\right)\mathbf{v}dx - \frac{1}{2}\int \mathbf{N}_v^{''\top} EI_{zz}\Theta_x\left(1+\frac{W_x^2}{6}\right)\mathbf{N}_w^{'}\mathbf{w}dx$$
$$-\frac{1}{2}\int \mathbf{N}_v^{''\top} EI_{zz}\sin^{-1}W_x\mathbf{N}_\theta^{'}\boldsymbol{\theta}dx = \int \mathbf{N}_v^\top\left(f_y - \frac{\partial m_z}{\partial x}\right)dx \quad (82)$$

The problem is cast as

$$\mathbf{K}(U, W, \Theta)\,\mathbf{x} = \mathbf{F} \quad (83)$$

where $\mathbf{x} = \begin{bmatrix}\mathbf{u}^\top & \mathbf{v}^\top & \mathbf{w}^\top & \boldsymbol{\theta}^\top\end{bmatrix}^\top$, $\mathbf{K}$ is the nonlinear stiffness matrix, and $\mathbf{F}$ is the force vector. The nonlinear global stiffness matrix and force vector are assembled from the following elemental stiffness matrix

and force vector:

$$\mathbf{k} = \begin{bmatrix} \mathbf{k}_{uu} & \mathbf{0} & \mathbf{k}_{uw} & \mathbf{k}_{u\theta} \\ \mathbf{0} & \mathbf{k}_{vv} & \mathbf{k}_{vw} & \mathbf{k}_{v\theta} \\ \mathbf{0} & \mathbf{0} & \mathbf{k}_{ww} & \mathbf{0} \\ \mathbf{0} & \mathbf{0} & \mathbf{0} & \mathbf{k}_{\theta\theta} \end{bmatrix} \tag{84}$$

$$\mathbf{f} = \int \begin{bmatrix} \mathbf{N}_u^\top f_x \\ \mathbf{N}_v^\top \left(f_y - \frac{\partial m_z}{\partial x} \right) \\ \mathbf{N}_w^\top \left(f_z + \frac{\partial m_y}{\partial x} \right) \\ \mathbf{N}_\theta^\top m_x \end{bmatrix} dx \tag{85}$$

where

$$\mathbf{k}_{uu} = \int \mathbf{N}_u^{'\top} EA \left(1 + \frac{1}{2} U_x \right) \mathbf{N}_u^{'} dx \tag{86}$$

$$\mathbf{k}_{uw} = \frac{1}{2} \int \mathbf{N}_u^{'\top} \left[EAW_x \left(1 + \frac{W_x^2}{6} \right)^2 \mathbf{N}_w^{'} + EI_{yy} \frac{W_{xx}}{1 - W_x^2} \mathbf{N}_w^{''} \right] dx \tag{87}$$

$$\mathbf{k}_{u\theta} = \frac{1}{2} \int \mathbf{N}_u^{'\top} EI_{xx} \Theta_x \mathbf{N}_\theta^{'} dx \tag{88}$$

$$\mathbf{k}_{vv} = \int \left(\mathbf{N}_v^{''\top} EI_{zz} \mathbf{N}_v^{''} dx + \mathbf{N}_v^{'\top} P_x \mathbf{N}_v^{'} \right) dx \tag{89}$$

$$\mathbf{k}_{vw} = -\frac{1}{2} \int \mathbf{N}_v^{''\top} EI_{zz} \Theta_x \left(1 + \frac{W_x^2}{6} \right) \mathbf{N}_w^{'} dx \tag{90}$$

$$\mathbf{k}_{v\theta} = -\frac{1}{2} \int \mathbf{N}_v^{''\top} EI_{zz} \sin^{-1} W_x \mathbf{N}_\theta^{'} dx \tag{91}$$

$$\mathbf{k}_{ww} = \int \left(\mathbf{N}_w^{''\top} EI_{yy} \frac{1 + U_x}{\sqrt{1 - W_x^2}} \mathbf{N}_w^{''} + \mathbf{N}_w^{'\top} P_x \mathbf{N}_w^{'} \right) dx \tag{92}$$

$$\mathbf{k}_{\theta\theta} = \int \mathbf{N}_\theta^{'\top} \left(GJ + P_x r_k^2 \right) \mathbf{N}_\theta^{'} dx \tag{93}$$

Note that the flapwise bending stiffness includes both the geometric nonlinear large deflection effect due to the term $\frac{1+U_x}{\sqrt{1-W_x^2}}$ and the nonlinear axial tension stiffening effect due to P_x which also exists in the torsional stiffness. The nonlinear large bending deflection effect thus increases the flapwise bending stiffness which effectively reduces the bending deflection.

The displacement matrix equation is nonlinear and can be solved for the static aeroelastic deflections by any nonlinear root search methods. One iterative method is proposed as follows:

- For $i = 0$, initialize $U_i(x) = 0$, $V_i(x) = 0$, $W_i(x) = 0$, and $\Theta_i(x) = 0$. Evaluate $\mathbf{K}_i$. Then, compute

$$\mathbf{x}_i = \mathbf{K}_i^{-1} \mathbf{F} \tag{94}$$

- For $i = 1, 2, \ldots, n$, evaluate $U_i(x)$, $V_i(x)$, $W_i(x)$, and $\Theta_i(x)$. Update $\mathbf{K}_i$. Then, iterate

$$\mathbf{x}_i = m\mathbf{x}_{i-1} + (1 - m) \mathbf{K}_i^{-1} \mathbf{F} \tag{95}$$

  with $0 \leq m < 1$ until $\mathbf{x}_i$ converges. Note that this algorithm will ensure numerical stability and converge to the 'exact' solution of Eq. (94) in the limit as $n \to \infty$. Equation (95) essentially imposes the stability condition on the unit circle. Otherwise, if Eq. (94) is used instead which corresponds to $m = 0$, numerical stability issues sometimes may be encountered. A suitable value for m is usually in the range between $\frac{1}{3}$ and $\frac{1}{2}$.

VI. Computational Results

A coupled aerodynamic-nonlinear finite element model is constructed for the CRM sub-scale model. The flow condition is at Mach 0.1162 and a dynamic pressure of 20 psf. The model is developed within a multidisciplinary coupled aerodynamic-nonlinear finite element analysis framework as shown in Fig. 10. The framework consists of four computational modules: 1) NASA vortex lattice code VORLAX[19] developed by Louis Miranda et al. with a pre-processor VORVIEW for providing a graphical user interface (GUI) for model geometry handling, 2) 2D Euler CFD code MSES with an integral boundary layer method developed by Mark Drela,[20] 3) an in-house computational geometry code that manipulates the model geometry deformation, and 4) an in-house nonlinear 3D beam finite element analysis (FEA) code with structural dynamics and aeroelasticity capabilities. The framework can compute the solution for a specified lift coefficient input or angle of attack input. For each solution for lift matching, VORLAX iteratively computes the angle of attack to match the specified lift coefficient. Then, the solution is corrected for the viscous and, if necessary, transonic flow effect with MSES which computes the lift and drag coefficients for each wing station in the VORLAX model. This transonic and viscous correction method requires an iteration loop between MSES and VORLAX. Once the corrections are made, VORLAX determines the new angle of attack iteratively to match the specified lift coefficient. At this point, the aerodynamic forces and moments are computed and then passed to the FEA code. The FEA code computes the wing deflections and then passes this deflection information to the computational geometry module which computes the geometry of the model deformation. This updated geometry is then passed to VORVIEW for geometry processing. The solution process is then repeated until the angle of attack converges to within a specified tolerance.

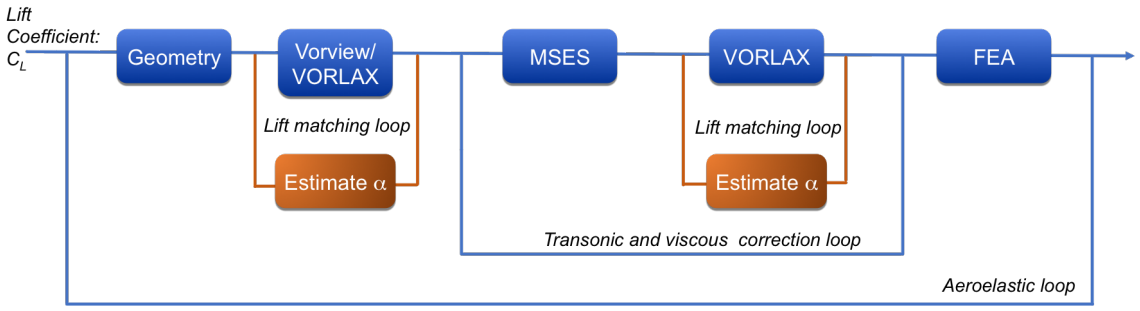

Figure 10. Coupled Aerodynamic-Nonlinear Finite Element Analysis Framework

Figure 11 shows the convergence of the iterative nonlinear solution according to Eq. (95) for three values of $m = 0, \frac{1}{3}, \frac{1}{2}$. The wing tip deflection W_t at the angle of attack of 7.616° is plotted as a function of the iteration number. The results show that the solution converges the fastest with $m = 0$ after only two iterations. As m increases, the convergence is slower. It is noted that in other situations where the nonlinear effects are much more dominant, experiences support the use of a positive value for m between $\frac{1}{3}$ and $\frac{1}{2}$.

Figure 12 shows the linear and nonlinear bending deflections of the CRM sub-scale model along the aircraft pitch axis y computed for the angle of attack of 9.538°. The linear deflection at the wing tip is 10.17 inches versus the nonlinear deflection of 10.11 inches. The wing length measured along the elastic axis is 99.69 inches. So the wing tip deflection is about 10% of the wing length. The nonlinear deflection is only slightly smaller than but essentially the same as the linear deflection.

Figure 13 shows the linear and nonlinear axial displacements of the CRM sub-scale model along the aircraft pitch axis y. The linear theory predicts an axial displacement of 0.01456 inches at the wing tip whereas the nonlinear theory predicts an axial displacement of -0.7124 inches. The axial extension with the linear theory is due to the drag force component along the swept elastic axis. As expected, the axial displacement computed by the linear theory is non-physical since it predicts a larger elongation of the wing than is possible. The linear theory predicts an elongation of 0.8396 inches as compared to the nonlinear theory which predicts an elongation of only 0.1136 inches due to the drag component along the elastic axis.

Figure 14 shows the linear and nonlinear chordwise bending deflections of the CRM sub-scale model along the aircraft pitch axis y. As expected, the chordwise bending deflections are very small due to the much

larger chordwise bending stiffness and the small drag force component acting normal to the elastic axis. Nonetheless, the difference between the linear and nonlinear bending theories is revealing. The nonlinear bending theory predicts a larger chordwise bending deflection but in the opposite direction than the linear bending theory. This is due to the contribution of the nonlinear term $\sin^{-1} W_x \Theta_x$ in Eq. (33) which causes a negative contribution to the chordwise bending deflection.

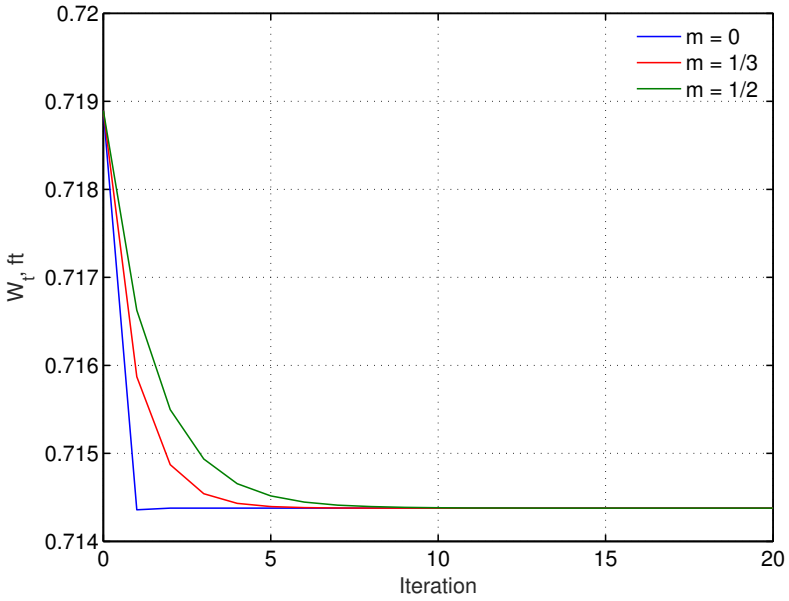

Figure 11. CRM Sub-Scale Model Solution Convergence at $\alpha = 7.616°$

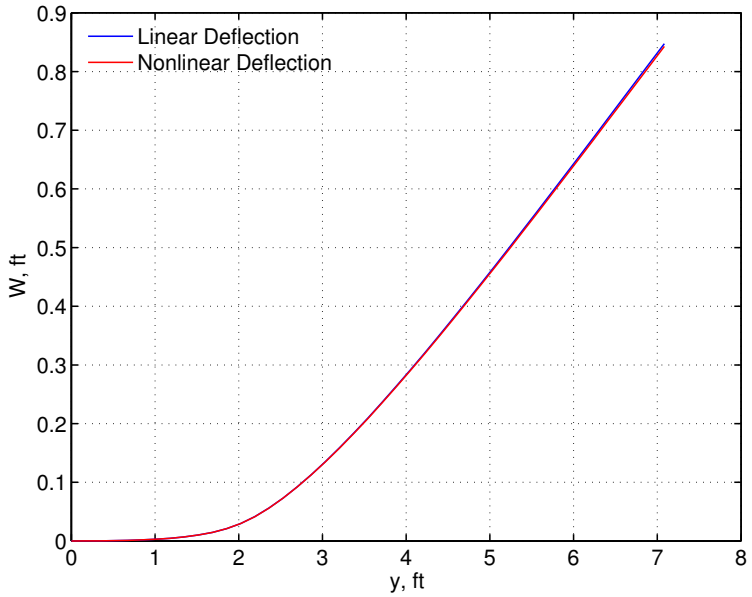

Figure 12. CRM Sub-Scale Model Flapwise Bending Deflection at $\alpha = 9.538°$

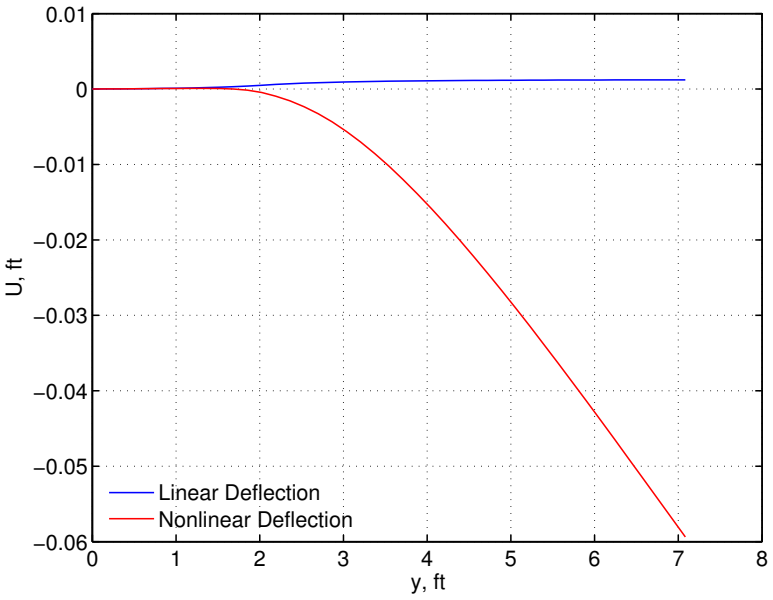

Figure 13. CRM Sub-Scale Model Axial Displacement at $\alpha = 9.538°$

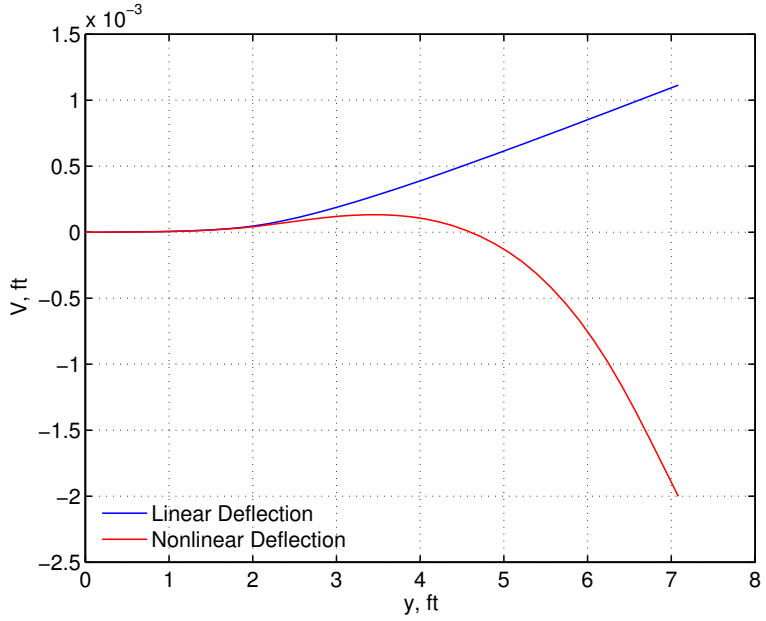

Figure 14. CRM Sub-Scale Model Chordwise Bending Deflection at $\alpha = 9.538°$

Figure 15 shows the linear and nonlinear torsional twists of the CRM sub-scale model along the aircraft pitch axis y. Both the linear and nonlinear torsional twists are virtually the same. The nonlinear theory

predicts a smaller torsional twist than the linear theory due to the presence of the small axial tension caused by the drag component along the elastic axis which acts to increase the torsional stiffness. This is observed in the results which show that the nonlinear torsional twist at the wing tip of $-0.5502°$ is slightly smaller than the linear torsional twist of $-0.5510°$.

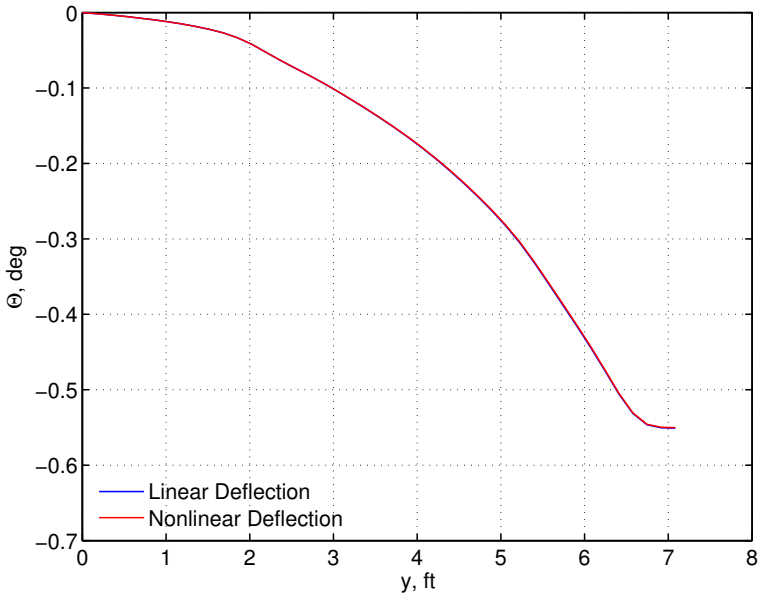

Figure 15. CRM Sub-Scale Model Torsional Twist at $\alpha = 9.538°$

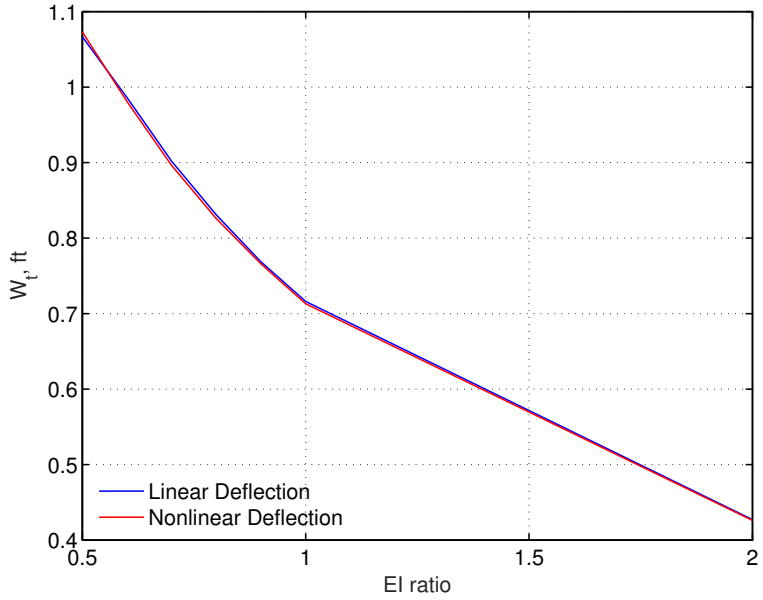

Figure 16. CRM Sub-Scale Model Flapwise Bending Deflection vs. Bending Stiffness

Figure 16 shows the effect of the flapwise bending stiffness on the linear and nonlinear bending deflections at the wing tip. The nonlinear bending deflection is generally smaller than the linear bending deflection, but as the stiffness is reduced by 50%, the trend is reverse. As the stiffness increases, the nonlinear and linear bending deflections appear to converge. This is expected because as the stiffness increases the bending deflection decreases until it is small enough that the linear bending theory holds.

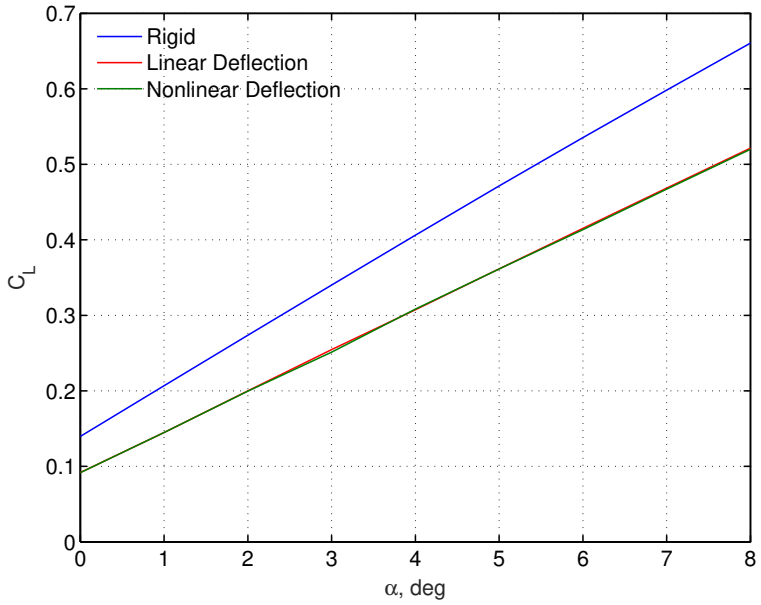

Figure 17. CRM Sub-Scale Drag Model Lift Coefficient vs. Angle of Attack at $M_\infty = 0.1162$

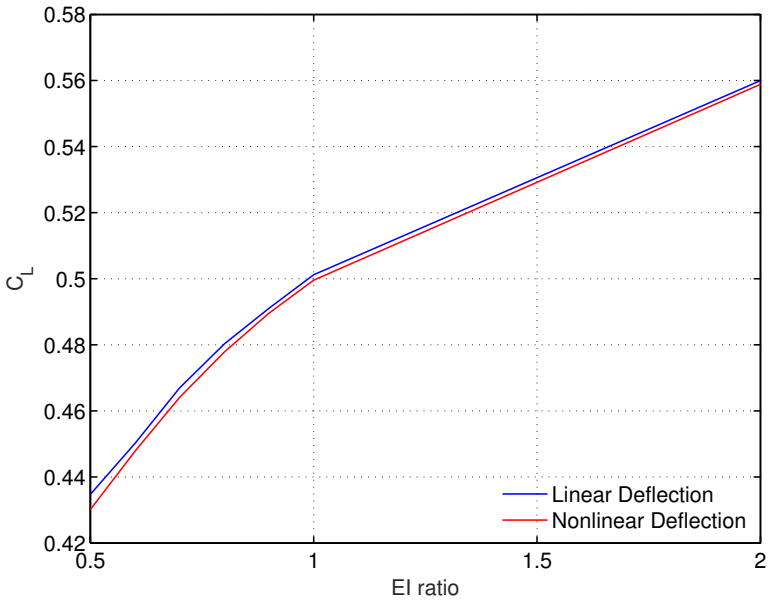

Figure 18. CRM Sub-Scale Drag Model Lift Coefficient at $\alpha = 7.616°$ and $M_\infty = 0.1162$ vs. Bending Stiffness

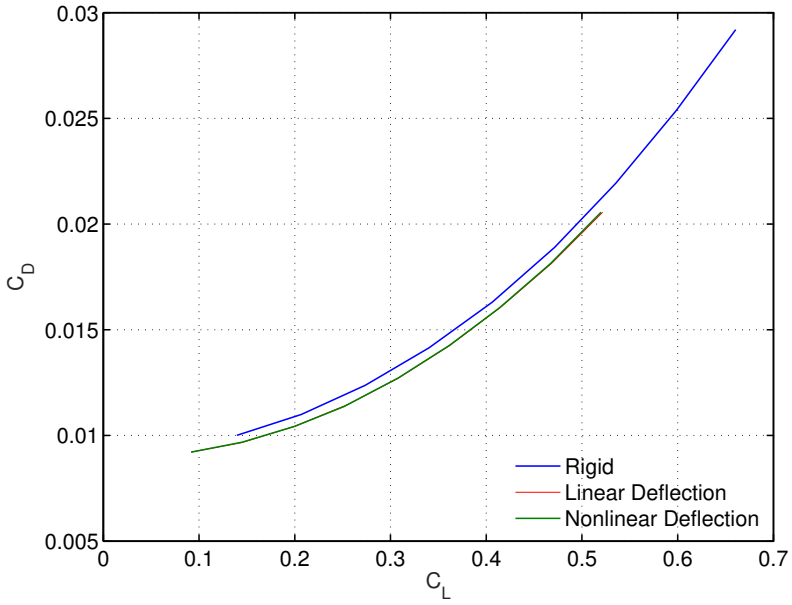

Figure 19. CRM Sub-Scale Model Drag Polar

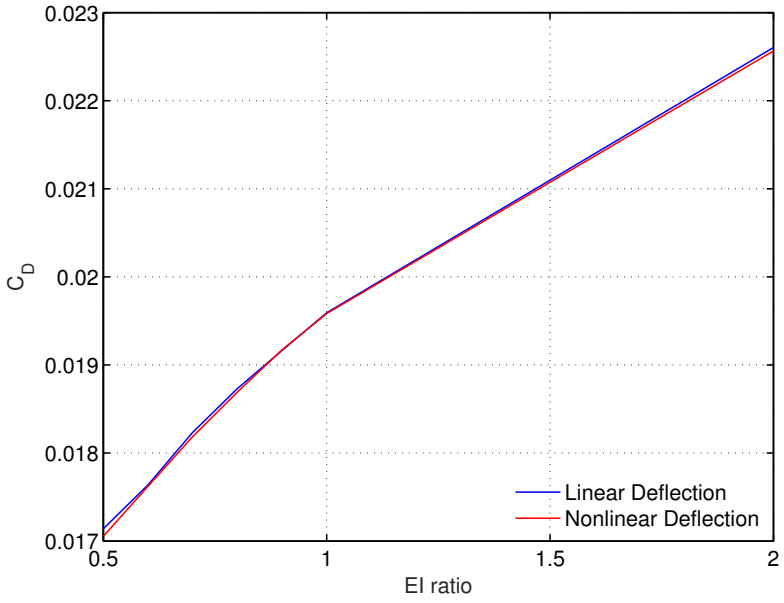

Figure 20. CRM Sub-Scale Model Drag Polar

Figure 17 shows the lift curves of the CRM sub-scale model. The rigid wing produces more lift at a given angle of attack than the flexible wing as expected. Both the linear and nonlinear bending deflections give

almost the same lift curves. On a closer look, the lift curve for the linear bending deflection is slightly higher than that for the nonlinear bending deflection. This becomes more apparent in Fig. 18. As the wing becomes stiffer, the difference in the lift coefficient between the nonlinear and linear bending deflection decreases.

Figure 19 shows the drag polar of the CRM sub-scale model. For the wind tunnel test, a jig shape twist optimization has been conducted to determine the optimal jig-shape twist that minimizes the induced drag for the CRM sub-scale model in its deflected state in the wind tunnel. As a result, at a fixed value of the lift coefficient, the rigid wing produces a higher drag than the flexible wing. The linear and nonlinear bending deflections both produce nearly identical drag coefficients. On a closer look, the drag coefficient for the nonlinear bending deflection appears to be slightly smaller than that for the linear bending deflection but not by much. At the angle of attack of 8°, the drag coefficients for the linear and nonlinear deflections are 0.020560 and 0.020557, respectively. Figure 20 shows that the drag coefficient for the nonlinear bending deflection is slightly lower than that for the linear bending deflection as the wing bending stiffness varies.

Figure 21 is the color map of the surface pressure distribution on the CRM sub-scale model.

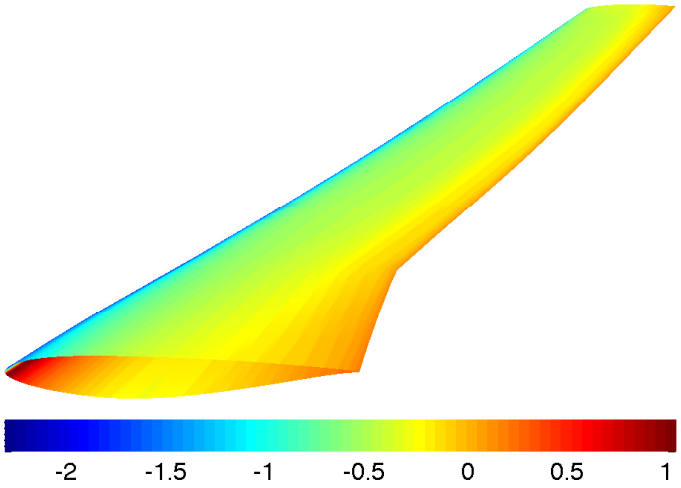

Figure 21. CRM Sub-Scale Model Surface Pressure Map at $\alpha = 7.616°$ and $M_\infty = 0.1162$

VII. Conclusions

This paper presents a nonlinear bending theory for large deflection bending. The nonlinear bending theory properly accounts for the length preservation when the structure is not subject to axial loading. While the linear bending theory predicts a similar bending deflection characteristic, it does not account correctly for the axial displacement. As a result, the linear bending theory is not length-preserving. At smaller bending deflections, the length-preserving property may not be significant, but when the bending deflection is sufficiently large, the nonlinear bending theory predicts a reduction in the wing span whereas the linear theory would fail to predict this effect. As a result, this could cause a significant effect on the wing aerodynamic performance. A modified lifting line theory is developed to take into account the full deflection states of the wing deformation. An analysis is conducted via an example of a high aspect ratio unswept wing to illustrate the effect of nonlinear large deflection bending on aerodynamics based on the lifting line theory. The results show that the nonlinear bending deflection causes a reduction in lift and span efficiency factor. The induced downwash for the ideal elliptical lift distribution cannot remain uniform across the wing span due to the bending deflection.

A coupled aerodynamic-nonlinear finite element model is developed for a Common Research Model (CRM) sub-scale wind tunnel model that will be tested at the University of Washington Aeronautical Laboratory to demonstrate an active real-time drag optimization control strategy. The computational results show that for this particular wind tunnel model there is a slight reduction in lift with the nonlinear bending theory, but otherwise the nonlinear bending theory does not have a dominant effect on the aerodynamic performance as compared to the linear bending theory. This study suggests that the linear bending theory is a good approach for analyzing this wind tunnel model.

Acknowledgment

The authors would like to acknowledge the Advanced Air Transport Technology Project under the Fundamental Aeronautics Program of NASA Aeronautics Research Mission Directorate (ARMD) for funding support of this work.

References

[1]Noll, T. E. and Eastep, F. E., "Active Flexible Wing Program," AIAA Journal of Aircraft, Vol. 32, No. 1, pp. 9-9, 1999.

[2]Pendleton, E., Flick, P., Voracek, D., Reichenbach, E., Griffin, K., and Paul, D., "The X-53,A Summary of the Active Aeroelastic Wing Flight Research Program," AIAA Structures, Structural Dynamics, and Materials Conference, AIAA-2007-1855, Honolulu, HI, April, 2007.

[3]Nguyen, N., "Elastically Shaped Future Air Vehicle Concept," NASA Innovation Fund Award 2010 Report, October 2010, Submitted to NASA Innovative Partnerships Program, http://ntrs.nasa.gov/archive/nasa/casi.ntrs.nasa.gov/20110023698.pdf.

[4]Nguyen, N., Trinh, K., Reynolds, K., Kless, J., Aftosmis, M., Urnes, J., and Ippolito, C., "Elastically Shaped Wing Optimization and Aircraft Concept for Improved Cruise Efficiency," 51st AIAA Aerospace Sciences Meeting, AIAA-2013-0141, January 2013.

[5]Urnes, J., Nguyen, N., Ippolito, C., Totah, J., Trinh, K., and Ting, E., "A Mission Adaptive Variable Camber Flap Control System to Optimize High Lift and Cruise Lift to Drag Ratios of Future N+3 Transport Aircraft," 51st AIAA Aerospace Sciences Meeting, AIAA-2013-0214, January 2013.

[6]Nguyen, N. and Urnes, J., "Aeroelastic Modeling of Elastically Shaped Aircraft Concept via Wing Shaping Control for Drag Reduction," AIAA Atmospheric Flight Mechanics Conference, AIAA-2012-4642, August 2012.

[7]Vassberg, J. C., DeHaan, M. C., Rivers, S. M., and Wahls, R. A., "Development of a Common Research Model for Applied CFD Validation Studies," AIAA Applied Aerodynamics Conference, AIAA 2008-6919, August 2008.

[8]Nguyen, N. and Ting, E., "Inertial Force Coupling to Nonlinear Aeroelasticity of Flexible Wing Aircraft," AIAA Dynamics Specialists Conference, AIAA-2016-1094, January 2016.

[9]Chaparro, D., Fujiwara, G., Ting, E., and Nguyen, N., "Aerodynamic Modeling of Transonic Aircraft Using Vortex Lattice Coupled with Transonic Small Disturbance for Conceptual Design," 34th AIAA Applied Aerodynamics Conference, AIAA-2016-3012, June 2016.

[10]Fujiwara, G., Chaparro, D., and Nguyen, N., "An Integral Boundary Layer Direct Method Applied to 2D Transonic Small-Disturbance Equations," 34th AIAA Applied Aerodynamics Conference, AIAA-2016-3160, June 2016.

[11]Nguyen, N., Ting, E., Nguyen, D., Dao, T., and Trinh, K., "Coupled Vortex Lattice Flight Dynamic Model with Aeroelastic Finite Element Model of Flexible Wing Transport Aircraft with Variable Camber Continuous Trailing Edge Flap for Drag Reduction," AIAA Atmospheric Flight Mechanics, AIAA-2013-4746, August 2013.

[12]Nguyen, N., "Integrated Flight Dynamics Modeling of Flexible Aircraft with Inertial Force-Propulsion - Aeroelastic Couplings," 46th AIAA Aerospace Sciences Meeting and Exhibit, AIAA-2008-0194, Reno, NV, January 2008.

[13]Houbolt, J. C. and Brooks, G. W., "Differential Equations of Motion for Combined Flapwise Bending, Chordwise Bending, and Torsion of Twisted Nonuniform Rotor Blades," NACA Technical Note 3905, February 1957.

[14]Hodges, D. W., "Proper Definition of Curvature in Nonlinear Beam Kinematics," AIAA Journal, Vol. 22, No. 12, 1984, pp. 1825-1827.

[15]Monasa, F. and Lewis, G., "Large Deflections of Point Loaded Cantilevers with Nonlinear Behavior," Journal of Applied Mathematics and Physics (ZAMP), Vol. 34, January 1983, pp. 124-130.

[16]Reddy, J. N. and Singh, I. R., "Large Deflections and Large-Amplitude Free Vibrations of Straight and Curved Beams," International Journal for Numerical Methods in Engineering, Vol. 17, 1981, pp. 829-852.

[17]Cones, C. D., "The Theory of Induced Lift and Minimum Induced Drag of Nonplanar Lifting Systems," NASA TR R-139, 1962.

[18]Nguyen, N., Ting, E., and Lebofsky, S., "Aeroelasticity of Axially Loaded Aerodynamic Structures for Truss-Braced Wing Aircraft," 56th AIAA/ASME/ASCE/AHS/ASC Structures, Structural Dynamics, and Materials Conference, AIAA-2015-1840, January 2015.

[19]Miranda, L. R., Elliott, R. D., and Baker, W. M., "A Generalized Vortex Lattice Method for Subsonic and Supersonic Flow Applications," NASA Contractor Report 2865, December 1977.

[20]Drela, M., "A User's Guide to MSES 3.05," MIT Department of Aeronautics and Astronautics, July 2007.